



CMS-SUS-16-044

 CERN-EP-2017-127
2018/02/12

Search for higgsino pair production in pp collisions at $\sqrt{s} = 13$ TeV in final states with large missing transverse momentum and two Higgs bosons decaying via $H \rightarrow b\bar{b}$

The CMS Collaboration^{*}

Abstract

Results are reported from a search for new physics in 13 TeV proton-proton collisions in the final state with large missing transverse momentum and two Higgs bosons decaying via $H \rightarrow b\bar{b}$. The search uses a data sample accumulated by the CMS experiment at the LHC in 2016, corresponding to an integrated luminosity of 35.9 fb^{-1} . The search is motivated by models based on gauge-mediated supersymmetry breaking, which predict the electroweak production of a pair of higgsinos, each of which can decay via a cascade process to a Higgs boson and an undetected lightest supersymmetric particle. The observed event yields in the signal regions are consistent with the standard model background expectation obtained from control regions in data. Higgsinos in the mass range 230–770 GeV are excluded at 95% confidence level in the context of a simplified model for the production and decay of approximately degenerate higgsinos.

Published in Physical Review D as doi:10.1103/PhysRevD.97.032007.

1 Introduction

The discovery of a Higgs boson [1–3] at the electroweak scale, with a mass $m_H \approx 125$ GeV [4–6], provides a new tool that can be used in searches for particles associated with physics beyond the standard model (SM). Particles predicted by models based on supersymmetry (SUSY) [7–14] are expected in many cases to decay into Higgs bosons with significant branching fractions, and in some cases, the presence of a Higgs boson can become a critical part of the experimental signature [15–19].

We perform a search for processes leading to Higgs boson pair production in association with large missing transverse momentum, p_T^{miss} . Each Higgs boson is reconstructed in its dominant decay mode, $H \rightarrow b\bar{b}$, which has a branching fraction of approximately 60%. Such a signature can arise, for example, in models based on SUSY, in which an electroweak process can lead to the production of two SUSY particles, each of which decays into a Higgs boson and another particle that interacts so weakly that it escapes detection in the apparatus. In this paper, we denote the particle in the search signature as H because it corresponds to the particle observed by ATLAS and CMS. However, in the context of SUSY models such as the minimal supersymmetric standard model (MSSM), this particle is usually assumed to correspond to the lighter of the two CP-even Higgs particles, denoted as h . The search uses an event sample of proton-proton (pp) collision data at $\sqrt{s} = 13$ TeV, corresponding to an integrated luminosity of 35.9 fb^{-1} , collected by the CMS experiment at the CERN LHC. Searches for this and related decay scenarios have been performed by ATLAS [19, 20] and CMS [15–17] using 7 and 8 TeV data. The analysis described here is based on an approach developed in Ref. [15].

While the observation of a Higgs boson completes the expected spectrum of SM particles, the low value of its mass raises fundamental questions that suggest the existence of new physics beyond the SM. Assuming that the Higgs boson is a fundamental (that is, noncomposite) spin-0 particle, stabilizing the electroweak scale (and the Higgs boson mass with it) is a major theoretical challenge, referred to as the gauge hierarchy problem [21–26]. Without invoking new physics, the Higgs boson mass would be pulled by quantum loop corrections to the cutoff scale of the theory, which can be as high as the Planck scale. Preventing such behavior requires an extreme degree of fine tuning of the theoretical parameters. Alternatively, stabilization of the Higgs boson mass can be achieved through a variety of mechanisms that introduce new physics at the TeV scale, such as SUSY.

The class of so-called natural SUSY models [27–31] contains the ingredients necessary to stabilize the electroweak scale. These models are the object of an intensive program of searches at the LHC. In any SUSY model, additional particles are introduced, such that all fermionic (bosonic) degrees of freedom in the SM are paired with corresponding bosonic (fermionic) degrees of freedom in the extended theory. In natural SUSY models, certain classes of partner particles are expected to be light. These include the four higgsinos ($\tilde{H}_{1,2}^0, \tilde{H}^\pm$); both top squarks, \tilde{t}_L and \tilde{t}_R , which have the same electroweak couplings as the left- (L) and right- (R) handed top quarks, respectively; the bottom squark with left-handed couplings (\tilde{b}_L); and the gluino (\tilde{g}). Of these, the higgsinos are generically expected to be the lightest. Furthermore, in natural scenarios, the four higgsinos are approximately degenerate in mass, so that transitions among these SUSY partners would typically produce only very soft (i.e., low momentum) additional particles, which would not contribute to a distinctive experimental signature.

In general, the gaugino and higgsino fields can mix, leading to mass eigenstates that are classified either as neutralinos ($\tilde{\chi}_i^0, i = 1–4$) or charginos ($\tilde{\chi}_i^\pm, i = 1–2$). If the $\tilde{\chi}_1^0$ is the lightest SUSY particle (LSP), it is stable in models that conserve R -parity [32] and, because of its weak

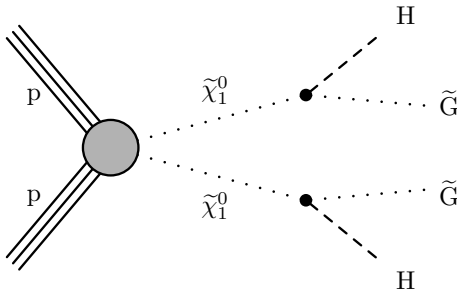


Figure 1: Diagram for the gauge-mediated symmetry breaking signal model, $\tilde{\chi}_1^0 \tilde{\chi}_1^0 \rightarrow HH\tilde{G}\tilde{G}$ (TChiHH), where \tilde{G} is a goldstino. The NLSPs $\tilde{\chi}_1^0$ are not directly pair produced, but are instead produced in the cascade decays of several different combinations of neutralinos and charginos, as described in the text.

interactions, would escape experimental detection. Achieving sensitivity to scenarios in which the higgsino sector is nearly mass degenerate and contains the LSP poses a significant experimental challenge because the events are characterized by low- p_T SM decay products and small values of p_T^{miss} [33–35]. Searches based on signatures involving initial-state radiation (ISR) recoiling against the pair produced higgsinos have already excluded limited regions of phase space for these scenarios [36–40]. However, achieving broad sensitivity based on this strategy is expected to require the large data samples that will be accumulated by the HL-LHC [41].

An alternative scenario arises, however, if the lightest higgsino/neutralino is not the LSP, but the next-to-lightest SUSY particle (NLSP) [42]. The LSP can be another particle that is generic in SUSY models, the goldstino (\tilde{G}). The goldstino is the Nambu–Goldstone particle associated with the spontaneous breaking of global supersymmetry and is a fermion. In a broad range of models in which SUSY breaking is mediated at a low scale, such as gauge-mediated supersymmetry breaking (GMSB) models [43, 44], the goldstino is nearly massless on the scale of the other particles and becomes the LSP. If SUSY is promoted to a local symmetry, as is required for the full theory to include gravity, the goldstino is “eaten” by the SUSY partner of the graviton, the gravitino ($J = 3/2$), and provides two of its four degrees of freedom. In the region of parameter space involving prompt decays to the gravitino, only the degrees of freedom associated with the goldstino have sufficiently large couplings to be relevant, so it is common to denote the LSP in either case as a goldstino. In these GMSB models, the goldstino mass is generically at the eV scale.

If the lighter neutralinos and charginos are dominated by their higgsino content and are thus nearly mass degenerate, their cascade decays can all lead to the production of the lightest neutralino, $\tilde{\chi}_1^0$ (now taken to be the NLSP), and soft particles. Integrating over the contributions from various allowed combinations of produced charginos and neutralinos ($\tilde{\chi}_1^0 \tilde{\chi}_2^0$, $\tilde{\chi}_1^0 \tilde{\chi}_1^\pm$, $\tilde{\chi}_2^0 \tilde{\chi}_1^\pm$, $\tilde{\chi}_1^\pm \tilde{\chi}_1^\mp$) therefore leads to an effective rate for $\tilde{\chi}_1^0 \tilde{\chi}_1^0$ production [45, 46] that is significantly larger than that for any of the individual primary pairs, resulting in a boost to the experimental sensitivity. The higgsino-like NLSP would then decay via $\tilde{\chi}_1^0 \rightarrow \gamma\tilde{G}$, $\tilde{\chi}_1^0 \rightarrow H\tilde{G}$, or $\tilde{\chi}_1^0 \rightarrow Z\tilde{G}$, where the goldstino can lead to large p_T^{miss} . The branching fractions for these decay modes vary depending on a number of parameters including $\tan\beta$, the ratio of the Higgs vacuum expectation values, and the branching fraction for $\tilde{\chi}_1^0 \rightarrow H\tilde{G}$ can be substantial. As a consequence, the signature $HH + p_T^{\text{miss}}$ with $H \rightarrow b\bar{b}$ can provide sensitivity to the existence of a higgsino sector in the important class of scenarios in which the LSP mass lies below the higgsino masses.

This article presents a search for higgsinos in events with $p_T^{\text{miss}} > 150$ GeV and at least three

jets identified as originating from b quark hadronization (b-tagged jets). In each event, we reconstruct two Higgs boson candidates and define search regions within a Higgs boson mass window. The background is dominated by $t\bar{t}$ production at low and intermediate p_T^{miss} , and by $Z \rightarrow \nu\bar{\nu}$ production in association with b quarks at high p_T^{miss} . The background is estimated entirely from data control regions corresponding to events with two b-tagged jets and events with three or four b-tagged jets outside the Higgs boson mass window. Systematic uncertainties on the background prediction are derived from both dedicated data control regions for $t\bar{t}$, $Z \rightarrow \nu\bar{\nu}$ and QCD multijet production as well as from the simulation of the background events in the search regions.

Results are interpreted in the simplified model framework [47–49] using the model shown in Fig. 1, hereafter referred to as TChiHH. In this model, two $\tilde{\chi}_1^0$ NLSPs are produced, each decaying via $\tilde{\chi}_1^0 \rightarrow H\tilde{G}$. The cross-section is calculated under the assumption that at least one of the $\tilde{\chi}_1^0$ NLSPs is produced in a cascade decay of $\tilde{\chi}_2^0$ or $\tilde{\chi}_1^\pm$, as described above. This situation arises when the mass splittings among charginos and neutralinos are large enough that the decays to $\tilde{\chi}_1^0$ occur promptly [50], while also small enough that the additional soft particles fall out of acceptance.

2 The CMS detector

The central feature of the CMS detector is a superconducting solenoid of 6 m internal diameter, providing a magnetic field of 3.8 T. Within the solenoid volume are the tracking and calorimeter systems. The tracking system, composed of silicon-pixel and silicon-strip detectors, measures charged particle trajectories within the pseudorapidity range $|\eta| < 2.5$, where $\eta \equiv -\ln[\tan(\theta/2)]$ and θ is the polar angle of the trajectory of the particle with respect to the counterclockwise proton beam direction. A lead tungstate crystal electromagnetic calorimeter (ECAL), and a brass and scintillator hadron calorimeter (HCAL), each composed of a barrel and two endcap sections, provide energy measurements up to $|\eta| = 3$. Forward calorimeters extend the pseudorapidity coverage provided by the barrel and endcap detectors up to $|\eta| = 5$. Muons are identified and measured within the range $|\eta| < 2.4$ by gas-ionization detectors embedded in the steel flux-return yoke outside the solenoid. The detector is nearly hermetic, permitting the accurate measurement of p_T^{miss} . A more detailed description of the CMS detector, together with a definition of the coordinate system used and the relevant kinematic variables, is given in Ref. [51].

3 Simulated event samples

Several simulated event samples are used for modeling the SM background and signal processes. While the background estimation in the analysis is performed from control samples in the data, simulated event samples are used to estimate uncertainties, as well as to build an understanding of the characteristics of the selected background events.

The production of $t\bar{t}$ +jets, W +jets, Z +jets, and quantum chromodynamics (QCD) multijet events is simulated with the Monte Carlo (MC) generator MADGRAPH5_aMC@NLO 2.2.2 [52] in leading-order (LO) mode [53]. Single top quark events are modeled with POWHEG v2 [54, 55] for the t -channel and tW production, and MADGRAPH5_aMC@NLO at next-to-leading order (NLO) [56] for the s -channel. Additional small backgrounds, such as $t\bar{t}$ production in association with bosons, diboson processes, and $t\bar{t}t\bar{t}$, are also produced at NLO with either MADGRAPH5_aMC@NLO or POWHEG. All events are generated using the NNPDF 3.0 [57] set of parton distribution functions. Parton showering and fragmentation are performed with the PYTHIA 8.205 [58] generator

with the underlying event model based on the CUETP8M1 tune [59]. The detector simulation is performed with GEANT4 [60–62]. The cross sections used to scale simulated event yields are based on the highest order calculation available [54, 55, 63–71], which for the most part correspond to NLO or next-to-NLO precision.

Signal events for the TChiHH simplified model are generated for 36 values of the higgsino mass between 127 and 1000 GeV. The mass points are denoted as TChiHH($m_{\tilde{\chi}_1^0}, m_{\tilde{G}}$), where $m_{\tilde{\chi}_1^0}$ is the higgsino mass and $m_{\tilde{G}}$ is the mass of the LSP, both in units of GeV. While the value of $m_{\tilde{G}}$ is fixed to 1 GeV in the simulation for technical reasons, the resulting event kinematics are consistent with an approximately massless LSP such as the goldstino in GMSB. The yields are normalized to the NLO + next-to-leading logarithmic (NLL) cross section [45, 46]. The production cross sections are calculated in the limit of mass degeneracy among higgsinos, $\tilde{\chi}_1^0, \tilde{\chi}_2^0$, and $\tilde{\chi}_1^\pm$. All other supersymmetric partners of the SM particles are assumed to be heavy (100 TeV) and thus essentially decoupled, a simplification that has a very small impact on higgsino pair production (e.g., the cross section changes less than 2% when the masses of the gluino and squarks are lowered down to 500 GeV). Following the convention of real mixing matrices and signed neutralino masses [72], we set the sign of the mass of $\tilde{\chi}_1^0$ ($\tilde{\chi}_2^0$) to +1 (−1). The lightest two neutralino states are defined as symmetric (anti-symmetric) combinations of higgsino states by setting the product of the elements N_{i3} and N_{i4} of the neutralino mixing matrix N to +0.5 (−0.5) for $i = 1$ (2). The elements U_{12} and V_{12} of the chargino mixing matrices U and V are set to 1. All chargino and neutralino decays in the simplified model are taken to be prompt, although the lifetimes of particles in a physical model would depend on the mass splitting between the higgsino-like states, which become long-lived in the limit of degenerate masses. Both Higgs bosons in each event are forced to decay to $b\bar{b}$, which is accounted for by scaling the signal event yields with the branching fraction of 58.24% [73]. The signal contribution from Higgs boson decays other than $H \rightarrow b\bar{b}$ is small in this analysis and is ignored. Signal events are generated in a manner similar to that for the SM backgrounds, with the MADGRAPH5_aMC@NLO 2.2.2 generator in LO mode using the NNPDF 3.0 set of parton distribution functions and followed by PYTHIA 8.205 for showering and fragmentation. The detector simulation is performed with the CMS fast simulation package [74] with scale factors applied to compensate for any differences with respect to the full simulation.

Finally, to model the presence of additional pp collisions from the same beam crossing as the primary hard-scattering process or another beam crossing adjacent to it (“pileup” interactions), the simulated events are overlaid with multiple minimum-bias events, which are also generated with the PYTHIA 8.205 generator with the underlying event model based on the CUETP8M1 tune.

4 Event reconstruction

4.1 Object definitions

The reconstruction of physics objects in an event proceeds from the candidate particles identified by the particle-flow (PF) algorithm [75], which uses information from the tracker, calorimeters, and muon systems to identify the candidates as charged or neutral hadrons, photons, electrons, or muons. The reconstructed vertex with the largest value of summed physics-object p_T^2 , with p_T denoting transverse momentum, is taken to be the primary pp interaction vertex (PV). The physics objects used in this context are the objects returned by a jet finding algorithm [76, 77] applied to all charged tracks associated with the vertex under consideration, plus the corresponding associated p_T^{miss} .

The charged PF candidates associated with the PV and the neutral PF candidates are clustered into jets using the anti- k_T algorithm [76] with a distance parameter $R = 0.4$, as implemented in the FASTJET package [77]. The jet momentum is determined as the vectorial sum of all particle momenta in the jet. Jet energy corrections are derived based on a combination of simulation studies, accounting for the nonlinear detector response and the presence of pileup, together with in situ measurements of the p_T balance in dijet and γ +jet events [78]. The resulting calibrated jet is required to satisfy $p_T > 30\text{ GeV}$ and $|\eta| \leq 2.4$. Additional selection criteria are applied to each event to remove spurious jet-like features originating from isolated noise in certain HCAL regions [79].

A subset of the jets are “tagged” as originating from b quarks using DEEPCSV [80], a new b tagging algorithm based on a deep neural network with four hidden layers [81]. We use all three of the DEEPCSV algorithm working points: loose, medium, and tight, defined by the values of the discriminator requirement for which the rates for misidentifying a light-flavor jet as a b jet are 10%, 1%, and 0.1%, respectively. The b tagging efficiency for jets with p_T in the 80–150 GeV range is approximately 86%, 69%, and 51% for the loose, medium, and tight working points, respectively, and gradually decreases for lower and higher jet p_T . The simulation is reweighted to compensate for any differences with respect to data based on measurements of the b tagging efficiency and mistag rate for each working point in dedicated data samples [80].

The missing transverse momentum, p_T^{miss} , is given by the magnitude of \vec{p}_T^{miss} , the negative vector sum of the transverse momenta of all PF candidates [82, 83], adjusted for known detector effects by taking into account the jet energy corrections. Filters are applied to reject events with well defined anomalous sources of p_T^{miss} arising from calorimeter noise, dead calorimeter cells, beam halo, and other effects.

Since the targeted signature is fully hadronic, contamination from final states involving leptons in the search region is suppressed by vetoing events with reconstructed lepton candidates. Electrons are identified by associating a charged particle track with an ECAL supercluster [84] and are required to have $p_T > 10\text{ GeV}$ and $|\eta| < 2.5$. Muons are identified by associating tracks in the muon system with those found in the silicon tracker [85] and are required to satisfy $p_T > 10\text{ GeV}$ and $|\eta| < 2.4$.

To preferentially consider only leptons that originate in the decay of W and Z bosons, leptons are required to be isolated from other PF candidates using an optimized version of the “mini-isolation” [86, 87]. The isolation I_{mini} is obtained by summing the transverse momentum of the charged hadrons, neutral hadrons, and photons within $\Delta R \equiv \sqrt{(\Delta\phi)^2 + (\Delta\eta)^2} < R_0$ of the lepton momentum vector \vec{p}^ℓ , where ϕ is the azimuthal angle in radians and R_0 is given by 0.2 for $p_T^\ell \leq 50\text{ GeV}$, $(10\text{ GeV})/p_T^\ell$ for $50 < p_T^\ell < 200\text{ GeV}$, and 0.05 for $p_T^\ell \geq 200\text{ GeV}$. Electrons (muons) are then required to satisfy $I_{\text{mini}}/p_T^\ell < 0.2$ (0.1).

As described in Section 5, the dominant background arises from the production of single-lepton $t\bar{t}$ events in which the lepton is a τ decaying hadronically, or is a light lepton that is either not reconstructed or fails the lepton selection criteria, including the p_T threshold and the isolation requirements. To reduce this background, we veto events with any additional isolated tracks corresponding to leptonic or hadronic PF candidates. To reduce the influence of tracks originating from pileup, isolated tracks are considered only if their closest distance of approach along the beam axis to a reconstructed vertex is smaller for the primary event vertex than for any other vertex.

The requirements for the definition of an isolated track differ slightly depending on whether the track is identified as leptonic or hadronic by the PF algorithm. For leptonic tracks, we

require $p_T > 5 \text{ GeV}$ and $I_{\text{trk}} < 0.2$, where I_{trk} is the scalar p_T sum of other charged tracks within $\Delta R < 0.3$ of the primary track, divided by the p_T value of the primary track. For hadronic tracks, we apply slightly tighter requirements to reduce hadronic (non- τ) signal loss: $p_T > 10 \text{ GeV}$ and $I_{\text{trk}} < 0.1$. To minimize the signal inefficiency due to this veto, isolated tracks are considered only if they are consistent with originating from a W boson decay, specifically, if the transverse mass of the track and the missing transverse momentum satisfy

$$m_T(\vec{p}_T^{\text{trk}}, \vec{p}_T^{\text{miss}}) \equiv \sqrt{2 p_T^{\text{trk}} p_T^{\text{miss}} [1 - \cos(\Delta\phi_{\vec{p}_T^{\text{trk}}, \vec{p}_T^{\text{miss}}})]} < 100 \text{ GeV}, \quad (1)$$

where \vec{p}_T^{trk} is the transverse momentum of the track and $\Delta\phi_{\vec{p}_T^{\text{trk}}, \vec{p}_T^{\text{miss}}}$ is the azimuthal separation between the track and \vec{p}_T^{miss} .

The majority of QCD multijet events containing high p_T^{miss} have at least one jet with undermeasured momentum and thus a spurious momentum imbalance. A signature of such an event is a jet closely aligned in direction with the \vec{p}_T^{miss} vector. To suppress this background, we place the following requirements on the angle $\Delta\phi_i$ between the i th highest p_T jet and \vec{p}_T^{miss} for $i = 1, 2, 3, 4$: $\Delta\phi_1 > 0.5$, $\Delta\phi_2 > 0.5$, $\Delta\phi_3 > 0.3$, and $\Delta\phi_4 > 0.3$. These conditions are hereafter collectively referred to as the high $\Delta\phi$ requirement.

The number of jets satisfying the criteria described above is denoted as N_{jets} , while the numbers of these jets tagged with the loose, medium, and tight b tagging working points are labeled as $N_{\text{b,L}}$, $N_{\text{b,M}}$, and $N_{\text{b,T}}$, respectively. By definition, the jets identified by each b tagging working point form a subset of those satisfying the requirements of looser working points.

4.2 Definition of b tag categories

To optimize signal efficiency and background rejection, we define the following mutually exclusive b tag categories:

- 2b category: $N_{\text{b,T}} = 2$, $N_{\text{b,M}} = 2$, $N_{\text{b,L}} \geq 2$,
- 3b category: $N_{\text{b,T}} \geq 2$, $N_{\text{b,M}} = 3$, $N_{\text{b,L}} = 3$, and
- 4b category: $N_{\text{b,T}} \geq 2$, $N_{\text{b,M}} \geq 3$, $N_{\text{b,L}} \geq 4$.

The 2b category is used as a control sample to determine the kinematic shape of the background. Most of the signal events lie in the 3b and 4b categories. This categorization is found to have superior performance with respect to other combinations of working points. For instance, the simpler option of only using medium b tags results in a 2b control sample that has a larger contribution from QCD multijet production and a 4b sample with smaller signal efficiency.

To study various sources of background with higher statistical precision, we also define the following b tag categories with looser requirements:

- 0b category: $N_{\text{b,M}} = 0$,
- 1b category: $N_{\text{b,M}} = 1$.

We will use N_{b} as a shorthand when discussing b tag categories as an analysis variable, and $N_{\text{b,L}}$, $N_{\text{b,M}}$, and $N_{\text{b,T}}$ when discussing numbers of b-tagged jets for specific working points.

4.3 Higgs boson pair reconstruction

The principal visible decay products in signal events are the four b jets from the decay of the two Higgs bosons. Additional jets may arise from initial- or final-state radiation as well as

pileup. To reconstruct both Higgs bosons, we choose the four jets with the largest DEEPCSV discriminator values, i.e., the four most b-quark-like jets. These four jets can be grouped into three different pairs of Higgs boson candidates. Of the three possibilities, we choose the one with the smallest mass difference Δm between the two Higgs boson candidate masses m_{H_1} and m_{H_2} ,

$$\Delta m \equiv |m_{H_1} - m_{H_2}|. \quad (2)$$

This method exploits the fact that signal events contain two particles of identical mass, without using the known value of the Higgs boson mass itself. Methods that use the known mass to select the best candidate tend to sculpt an artificial peak in the background.

Only events where the masses of the two Higgs boson candidates are similar, $\Delta m < 40\text{ GeV}$, are kept. We then calculate the average mass as

$$\langle m \rangle \equiv \frac{m_{H_1} + m_{H_2}}{2}. \quad (3)$$

As discussed in Section 6, the search is then performed within the Higgs boson mass window defined as $100 < \langle m \rangle \leq 140\text{ GeV}$.

After selecting the two Higgs boson candidates, we compute the distance ΔR between the two jets in each of the $H \rightarrow b\bar{b}$ candidate decays. We then define ΔR_{\max} as the larger of these two values,

$$\Delta R_{\max} \equiv \max(\Delta R_{H_1}, \Delta R_{H_2}). \quad (4)$$

In the typical configuration of signal events satisfying the baseline requirements, ΔR_{\max} is small because the Higgs bosons tend to have nonzero transverse boost and, thus, the two jets from the decay of a Higgs boson tend to lie near each other in η and ϕ . In contrast, for semileptonic $t\bar{t}$ background events, three of the jets typically arise from a top quark that decays via a hadronically decaying W boson while the fourth jet arises from a b quark from the other top quark decay. Therefore, three of the jets tend to lie within the same hemisphere while the fourth jet is in the opposite hemisphere. One of the Higgs boson candidates is thus formed from jets in both hemispheres, and ΔR_{\max} tends to be larger than it is for signal events.

5 Trigger and event selection

The data sample was obtained with triggers that require the online p_T^{miss} value to be greater than 100 to 120 GeV, the applied threshold varying with the instantaneous luminosity delivered by the LHC. This variable is computed with trigger-level quantities, and therefore has somewhat worse resolution than the corresponding offline variable. The trigger efficiency measured as a function of offline p_T^{miss} , in samples triggered by a high- p_T isolated electron, rises rapidly from about 60% at $p_T^{\text{miss}} = 150\text{ GeV}$ to 92% for $p_T^{\text{miss}} = 200\text{ GeV}$ and to over 99% for $p_T^{\text{miss}} > 300\text{ GeV}$. The systematic uncertainty in the trigger efficiency is obtained by comparing the nominal efficiency with that found in different kinematic regions, with various reference triggers, and with the simulation. This uncertainty is about 7% for $p_T^{\text{miss}} = 150\text{ GeV}$ and decreases to 0.7% for $p_T^{\text{miss}} > 300\text{ GeV}$.

Several data control samples are employed to validate the analysis techniques and to estimate systematic uncertainties in the background estimates. The control sample for the principal background from $t\bar{t}$ events requires exactly one electron or one muon, while the $Z \rightarrow \nu\bar{\nu}$ background is studied with a control sample requiring two leptons consistent with a $Z \rightarrow \ell^+\ell^-$ decay. These data samples were obtained with triggers that require at least one electron or muon with p_T greater than 27 or 24 GeV, respectively.

Signal events have four b jets from the decay of two Higgs bosons and no isolated leptons, with any additional hadronic activity coming from initial- or final-state radiation. Thus, we select events with four or five jets, no leptons or isolated tracks, $N_{b,T} \geq 2$, $p_T^{\text{miss}} > 150 \text{ GeV}$, high $\Delta\phi$, $\Delta m < 40 \text{ GeV}$, and $\Delta R_{\text{max}} < 2.2$. These selection requirements, listed in the top half of Table 1, are referred to as the *baseline selection*, while the bottom half of that table shows the further reduction in background in increasingly more sensitive search bins. The distributions of Δm , ΔR_{max} , and $\langle m \rangle$ in the 4b category are shown in Fig. 2 in data and simulation. The actual background prediction, however, is based on data control samples, as described in the next section.

Table 1: Event yields obtained from simulated event samples scaled to an integrated luminosity of 35.9 fb^{-1} , as the event selection criteria are applied. The category “ $t\bar{t}+X$ ” is dominated by $t\bar{t}$ (98.5%), but also includes small contributions from $t\bar{t}t\bar{t}$, $t\bar{t}W$, $t\bar{t}Z$, $t\bar{t}H$, and $t\bar{t}\gamma$ backgrounds. The category “V+jets” includes Z+jets and W+jets backgrounds in all their decay modes. The category “Other” includes ZZ, WZ, WW, WH($\rightarrow b\bar{b}$), and ZH($\rightarrow b\bar{b}$) processes. The event selection requirements listed up to and including $\Delta R_{\text{max}} < 2.2$ are defined as the *baseline selection*. The trigger efficiency is applied as an event weight and is first taken into account in the $p_T^{\text{miss}} > 150 \text{ GeV}$ row. The uncertainties in the “Total SM bkg.” column is statistical only. The columns corresponding to the yields for three signal benchmark points are labeled by TChiHH($m_{\tilde{\chi}_1^0}, m_{\tilde{G}}$), with $m_{\tilde{\chi}_1^0}$ and $m_{\tilde{G}}$ in units of GeV. The simulated samples for TChiHH(225,1), TChiHH(400,1), and TChiHH(700,1) are equivalent to 10, 100, and over 1000 times the data sample, respectively, so the statistical uncertainties in the signal yields are small.

$\mathcal{L} = 35.9 \text{ fb}^{-1}$	Other	Single t	QCD	V+jets	$t\bar{t}+X$	Total SM bkg.	TChiHH (225,1)	TChiHH (400,1)	TChiHH (700,1)
No selection	—	—	—	—	—	—	10477.0	1080.3	84.0
0ℓ , 4–5 jets	—	—	—	—	—	—	4442.0	544.9	44.6
$N_{b,T} \geq 2$	—	—	—	—	—	—	2509.3	308.9	23.9
$p_T^{\text{miss}} > 150 \text{ GeV}$	122.3	1847.0	13201.4	2375.8	26797.7	44344.2 ± 778.5	509.5	204.2	20.4
Track veto	91.4	1130.1	12251.8	1987.0	16910.1	32370.5 ± 770.5	476.9	196.3	19.9
High $\Delta\phi$	62.3	688.4	1649.0	1466.6	12027.0	15893.4 ± 482.6	267.2	162.3	17.5
$ \Delta m < 40 \text{ GeV}$	35.9	366.0	831.9	745.5	7682.3	9661.6 ± 440.8	191.8	119.4	12.2
$\Delta R_{\text{max}} < 2.2$	14.2	138.2	147.0	336.9	3014.2	3650.5 ± 90.2	98.3	79.6	10.1
$100 < \langle m \rangle \leq 140 \text{ GeV}$	3.8	42.3	14.0	75.2	992.0	1127.3 ± 10.1	72.9	61.0	8.3
3b + 4b	0.1	3.4	3.2	7.1	109.0	122.9 ± 3.9	54.9	46.5	6.3
4b	0.1	0.7	3.2	1.5	27.3	32.8 ± 3.4	38.1	32.8	4.6
$p_T^{\text{miss}} > 200 \text{ GeV}$	0.1	0.3	3.2	1.1	9.4	14.1 ± 3.3	16.2	27.4	4.3
$p_T^{\text{miss}} > 300 \text{ GeV}$	0.0	0.1	0.0	0.4	1.1	1.7 ± 0.2	2.0	11.5	3.5
$p_T^{\text{miss}} > 450 \text{ GeV}$	0.0	0.0	0.0	0.1	0.1	0.1 ± 0.1	0.0	1.1	2.0

Based on the simulation, after the baseline selection, more than 85% of the remaining SM background arises from semileptonic $t\bar{t}$ production. Approximately half of this contribution corresponds to $t\bar{t}$ events with an electron or a muon in the final state that is either out of acceptance or not identified, while the other half involves final states with a hadronically decaying τ lepton. The contributions from events with a W or Z boson in association with jets (V+jets) are about 10% and are dominated by $Z \rightarrow \nu\bar{\nu}$ decays. The background from QCD multijet events after the baseline selection is very small due to the combination of p_T^{miss} , $\Delta\phi$, and N_b requirements.

As shown in Fig. 2, the p_T^{miss} distribution of the signal is highly dependent on the higgsino mass. To further enhance the sensitivity of the analysis, we therefore subdivide the search region into four p_T^{miss} bins: $150 < p_T^{\text{miss}} \leq 200 \text{ GeV}$, $200 < p_T^{\text{miss}} \leq 300 \text{ GeV}$, $300 < p_T^{\text{miss}} \leq 450 \text{ GeV}$, and $p_T^{\text{miss}} > 450 \text{ GeV}$. The background estimation procedure described in Section 6 is then applied separately in each of the four p_T^{miss} bins.

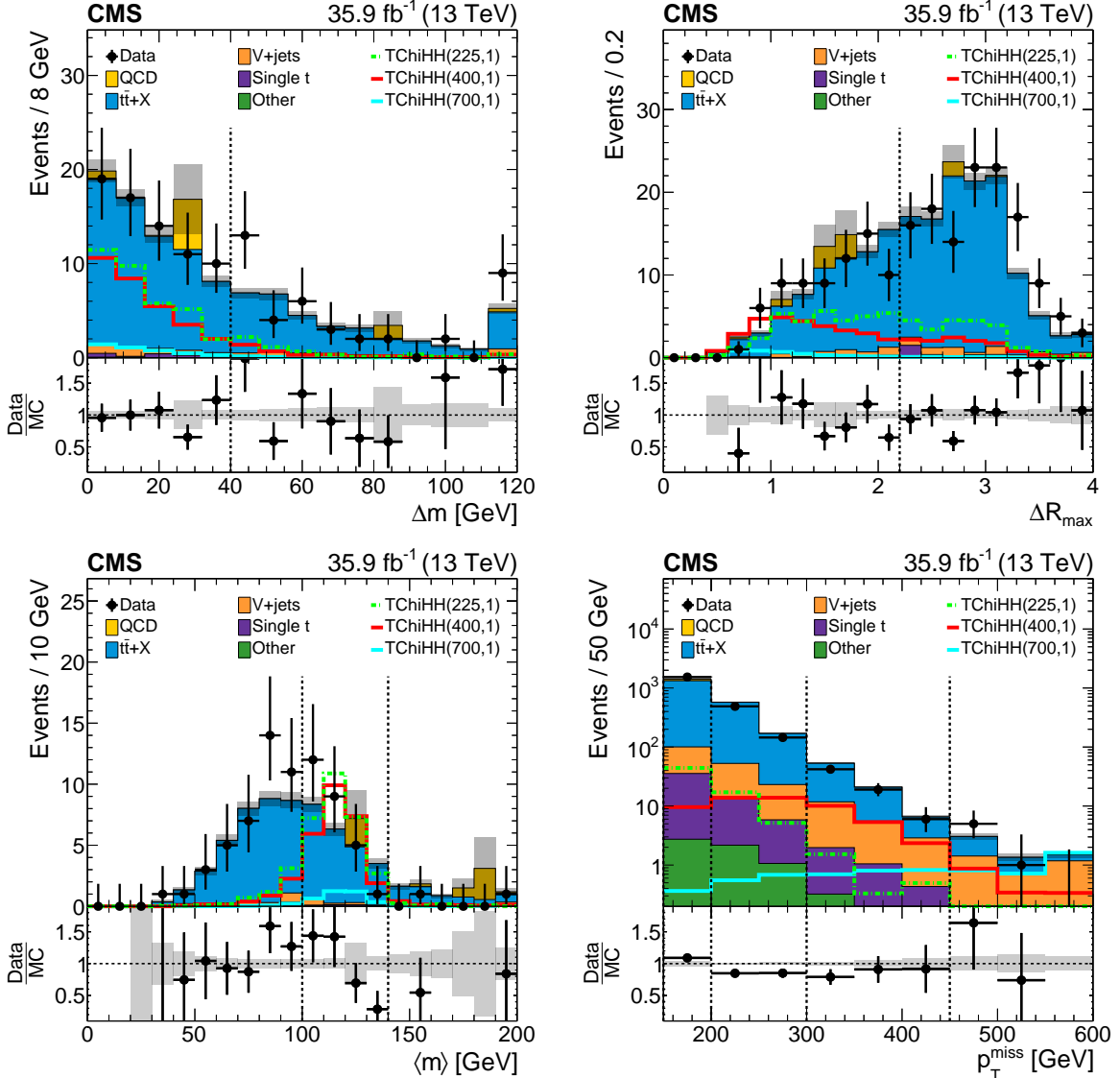


Figure 2: Distributions of Δm , ΔR_{\max} , $\langle m \rangle$, and p_T^{miss} for data and simulated background samples, as well as three signal benchmark points denoted as TChiHH($m_{\tilde{\chi}_1^0}, m_{\tilde{G}}$), with $m_{\tilde{\chi}_1^0}$ and $m_{\tilde{G}}$ in units of GeV. All figures include baseline requirements (except on the variable being plotted in the case of Δm and ΔR_{\max}). The Δm , $\langle m \rangle$, and ΔR_{\max} distributions also include the 4b selection. The simulation is normalized to the observed data yields. The gray shading indicates the statistical uncertainty in the total simulated background. The vertical dotted lines indicate baseline requirements in the top row figures, the search region mass window in $\langle m \rangle$ in the bottom left figure, and the p_T^{miss} binning in the bottom right figure. The last bin includes overflow.

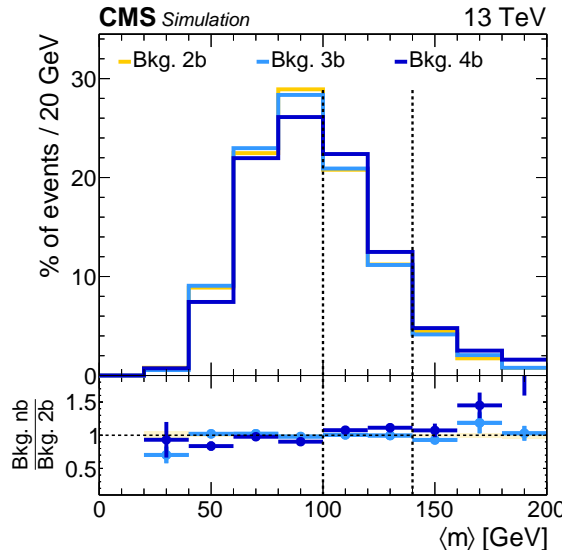


Figure 3: Distribution of $\langle m \rangle$ after the baseline selection, showing the agreement between the $\langle m \rangle$ shapes among the three b tag categories. The comparison is based on simulation including all backgrounds except QCD multijet production, for which the simulation suffers from large statistical uncertainties. QCD multijet events account for less than 5% of the total yield. The vertical dotted lines indicate the Higgs boson mass window.

6 Background estimation

6.1 Method

The background estimation method is based on the observation that the $\langle m \rangle$ distribution is approximately uncorrelated with the number of b tags. As shown in Fig. 3, the $\langle m \rangle$ shapes for the three b tag categories agree within the statistical uncertainty in the simulated samples. This behavior can be understood by noting that the background in all three b tag categories is dominated by events containing only two b quarks, with the additional b-tagged jets in the 3b and 4b categories being mistagged light-flavor or gluon jets. The background simulation indicates that only 20% (37%) of the events in the 3b (4b) selection have more than two b quarks. As a result, the four jets used to construct $\langle m \rangle$ in the 3b and 4b categories arise largely from the same fundamental processes as those with two b-tagged jets, and thus the shape of the average mass distribution is independent of N_b for $N_b \geq 2$.

Taking advantage of this observation, we estimate the background contribution to each signal bin with an ABCD method [87] that employs $\langle m \rangle$ and the b tag categories as the two ABCD variables similarly to the 8 TeV analysis [15]. We define the Higgs boson mass window (HIG region) as the events with $\langle m \rangle$ within 100 to 140 GeV, and the Higgs boson mass sideband (SBD region) as the events with $0 < \langle m \rangle < 100$ GeV or $140 < \langle m \rangle < 200$ GeV. The mass window is chosen to optimize the signal sensitivity, taking into account the background distribution and the asymmetry in the Higgs boson mass resolution. The 3b and 4b SBD regions, together with the shape of the $\langle m \rangle$ distribution in the 2b category, are then used to determine the background in the signal-enriched 3b and 4b HIG regions independently for each p_T^{miss} bin as follows:

$$\mu_{\text{HIG},3b}^{\text{bkg}} = R \mu_{\text{SBD},3b}^{\text{bkg}} \quad \text{and} \quad \mu_{\text{HIG},4b}^{\text{bkg}} = R \mu_{\text{SBD},4b}^{\text{bkg}}. \quad (5)$$

Here, $\mu_{\text{SBD},nb}^{\text{bkg}}$ and $\mu_{\text{HIG},nb}^{\text{bkg}}$ are the background rates for each b tag category ($n = 2, 3, 4$) in the SBD and HIG search regions, respectively, and R is the ratio of the background rate in the HIG

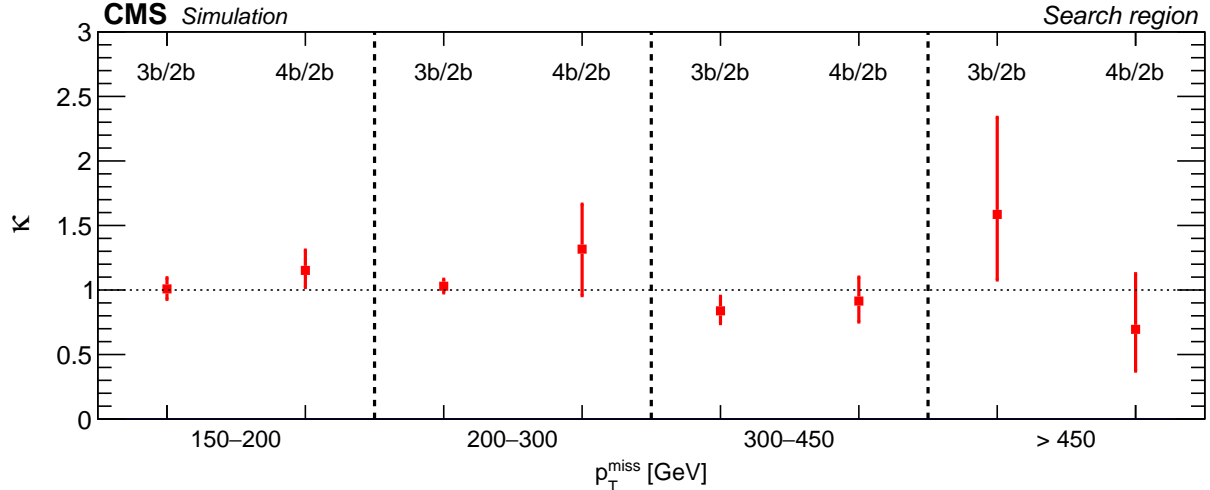


Figure 4: Values of the double ratios $\kappa_{3\text{b}}$ and $\kappa_{4\text{b}}$ obtained from the background simulation for each of the p_T^{miss} bins. The error bars correspond to the statistical uncertainty of the background simulation.

region to that in the SBD region. In the limit that the b tag category and $\langle m \rangle$ are uncorrelated, R is the same for the three b tag categories:

$$R \equiv \left(\frac{\mu_{\text{HIG}}^{\text{bkg}}}{\mu_{\text{SBD}}^{\text{bkg}}} \right)_{2\text{b}} = \left(\frac{\mu_{\text{HIG}}^{\text{bkg}}}{\mu_{\text{SBD}}^{\text{bkg}}} \right)_{3\text{b}} = \left(\frac{\mu_{\text{HIG}}^{\text{bkg}}}{\mu_{\text{SBD}}^{\text{bkg}}} \right)_{4\text{b}}. \quad (6)$$

The *closure* of the background estimation method, that is, the ability of Eq. (5) to predict the background rates in the signal regions, is quantified with the double ratios

$$\kappa_{3\text{b}} = \left(\frac{\mu_{\text{HIG}}^{\text{bkg}}}{\mu_{\text{SBD}}^{\text{bkg}}} \right)_{3\text{b}} / \left(\frac{\mu_{\text{HIG}}^{\text{bkg}}}{\mu_{\text{SBD}}^{\text{bkg}}} \right)_{2\text{b}} \quad \text{and} \quad \kappa_{4\text{b}} = \left(\frac{\mu_{\text{HIG}}^{\text{bkg}}}{\mu_{\text{SBD}}^{\text{bkg}}} \right)_{4\text{b}} / \left(\frac{\mu_{\text{HIG}}^{\text{bkg}}}{\mu_{\text{SBD}}^{\text{bkg}}} \right)_{2\text{b}}. \quad (7)$$

These κ factors measure the impact of any residual correlation between the b tag category and $\langle m \rangle$. Figure 4 shows that the κ factors in simulation are consistent with unity for both the 3b and 4b regions across the full p_T^{miss} range, demonstrating the validity of the fundamental assumption of the ABCD method. In Section 7, we study the closure of the method in data control samples and estimate the associated systematic uncertainties in the background prediction.

6.2 Implementation

The method outlined in Section 6.1 is implemented with a likelihood function that incorporates the statistical and systematic uncertainties associated with the background prediction and the signal model, and also accounts for signal contamination in all control regions.

The terms in the likelihood function corresponding to the observed yields in all analysis regions, reflecting the parameterization of the ABCD method and the signal contributions to each bin, can be written as the following product of Poisson probability density functions (pdfs):

$$\begin{aligned} \mathcal{L}_{\text{ABCD}} = & \prod_{m=1}^4 \prod_{n=2}^4 \text{Poisson}(N_{\text{SBD},nb,m}^{\text{data}} | \mu_{\text{SBD},nb,m}^{\text{bkg}} + r \mu_{\text{SBD},nb,m}^{\text{sig}}) \\ & \times \prod_{m=1}^4 \prod_{n=2}^4 \text{Poisson}(N_{\text{HIG},nb,m}^{\text{data}} | R \mu_{\text{SBD},nb,m}^{\text{bkg}} + r \mu_{\text{HIG},nb,m}^{\text{sig}}). \end{aligned} \quad (8)$$

Here, the index m runs over the four p_T^{miss} bins, the index n runs over the three b tag categories, N^{data} are the observed data yields, μ^{sig} are the expected signal rates, and r is the parameter quantifying the signal strength relative to the expected yield across all analysis bins. The four main floating parameters describing the fitted background for each p_T^{miss} bin m are the three sideband background rates $\mu_{\text{SBD},nb,m}^{\text{bkg}}$ and the ratio R .

The full likelihood function is given by the product of $\mathcal{L}_{\text{ABCD}}$, Poisson pdfs constraining the signal shape and its statistical uncertainty in each bin, and log-normal pdfs constraining nuisance parameters that account for the systematic uncertainties in the closure and the signal efficiency. These nuisance parameters were omitted from Eq. (8) for simplicity.

Following the approach in Ref. [87], the likelihood function is employed in two types of fits: the *predictive fit*, which allows us to more easily establish the agreement of the background predictions and the observations in the background-only hypothesis, and the *global fit*, which enables us to estimate the signal strength.

The predictive fit is realized by removing the terms of the likelihood corresponding to the observed yields in the signal regions, (HIG, 3b) and (HIG, 4b), and fixing the signal strength r to 0. As a result, we obtain a system of equations with an equal number of unknowns and constraints. For each p_T^{miss} bin, the four main floating parameters $\mu_{\text{SBD},2b}^{\text{bkg}}$, $\mu_{\text{SBD},3b}^{\text{bkg}}$, $\mu_{\text{SBD},4b}^{\text{bkg}}$, and R are determined by the four observations $N_{\text{SBD},2b}^{\text{data}}$, $N_{\text{SBD},3b}^{\text{data}}$, $N_{\text{SBD},4b}^{\text{data}}$, and $N_{\text{HIG},2b}^{\text{data}}$. Since the extra floating parameters corresponding to the systematic uncertainties are constrained by their respective log-normal pdfs, they do not contribute as additional degrees of freedom. The predictive fit thus converges to the standard ABCD method, and the likelihood maximization machinery becomes just a convenient way to solve the system of equations and to propagate the various uncertainties.

Conversely, the global fit includes the observations in the signal regions. Since in this case there are six observations and four floating background parameters in each p_T^{miss} bin, there are enough constraints for the signal strength r to be determined in the fit. The global fit also properly accounts for the signal yields in the control regions, using the signal shape across control and signal regions from the simulation.

7 Systematic uncertainties in the background prediction

The background estimation procedure described in Section 6 relies on the approximate independence of the $\langle m \rangle$ and N_b distributions. In Sections 7.1, 7.2, and 7.3 we study this assumption for individual background processes in data and simulation by defining dedicated control regions for $t\bar{t}$, Z+jets, and QCD multijet production. The overall level of closure in these control samples, better than 13% in all cases, is assigned as a systematic uncertainty for each of the main background sources separately. Additionally, these samples validate the closure in the simulation as a function of p_T^{miss} .

If the background estimation method is valid for each separate background contribution, then it would also be valid for the full background composition as long as the relative abundance of each background component is independent of N_b . In Section 7.4, we use these data control samples to quantify the validity of the simulation prediction that the background composition is independent of N_b in each p_T^{miss} bin by examining the modeling of the p_T^{miss} and N_b distributions for each background source.

Finally, in Section 7.5, we describe the prescription for assigning the total systematic uncer-

tainty in the background prediction binned in p_T^{miss} and N_b , taking into account both the findings from the data control sample studies and the closure of the method in the simulation. The latter is the dominant systematic uncertainty in this analysis.

7.1 Single-lepton $t\bar{t}$ control sample

To test whether the background estimation method works for $t\bar{t}$ events, we define a single-lepton control sample, which, like the search region, is dominated by single-lepton $t\bar{t}$ events and represents a similar kinematic phase space. Because the lepton is a spectator object as far as the ABCD method is concerned—it is neither involved in the construction of the $\langle m \rangle$ variable, nor correlated with the presence of additional b tags—this control sample should accurately capture any potential mismodeling of the $\langle m \rangle$ - N_b correlation that may be present in the signal region. While this control region does not specifically probe semileptonic $t\bar{t}$ events involving a hadronically decaying τ lepton, the simulation shows that their $\langle m \rangle$ distribution in the signal region is the same as that of semileptonic $t\bar{t}$ events involving light leptons. This is expected because in most cases the τ lepton in these events is either out of acceptance or reconstructed as the jet with the smallest b-discriminator value and, as a result, it does not enter the $\langle m \rangle$ calculation.

For each of the four p_T^{miss} search bins, we construct a corresponding ABCD test in a single-lepton control sample, defined by the same selection requirements except for removing the lepton and the isolated track vetoes and instead requiring exactly one lepton with $p_T > 30 \text{ GeV}$ (to reach trigger efficiency plateau) and $m_T(\vec{p}_T^\ell, \vec{p}_T^{\text{miss}}) < 100 \text{ GeV}$ (to avoid poorly reconstructed events). Given that the contamination from QCD multijet production in the single-lepton region is small, the $\Delta\phi$ requirement is also removed to further improve the statistical power of the control sample. Since the lepton provides a way to trigger on events with lower p_T^{miss} , we add two additional p_T^{miss} bins, $p_T^{\text{miss}} < 75 \text{ GeV}$ and $75 < p_T^{\text{miss}} \leq 150 \text{ GeV}$, allowing us to study the p_T^{miss} dependence of the closure in a wider range. In this control region, $t\bar{t}$ production accounts for over 90% of the events, except for the two highest p_T^{miss} bins, where the total contribution of single top quark and V+jets production can be as high as $\sim 25\%$. Figure 5 (left) shows the comparison of the $\langle m \rangle$ shapes between the data and the simulation.

As described in Section 6, since the 3b and 4b categories are dominated by events with two true B hadrons and one or two additional mistagged jets, similar jet topologies contribute to all b tag categories and thus the $\langle m \rangle$ distributions of the reconstructed b tag categories converge. We validate this assertion in the single-lepton control sample by examining the value of the κ factors. Figure 6 shows the overall closure of the method across bins of p_T^{miss} , both in the simulation and in data. We observe agreement within the statistical uncertainties, with κ values being consistent with unity across the full p_T^{miss} range for both data and simulation. This observation is also confirmed with larger statistical precision by repeating the test in a more inclusive sample obtained by removing the ΔR_{max} requirement.

An overall uncertainty in the validity of the method in $t\bar{t}$ -like events is assigned based on the larger of the nonclosure and the statistical uncertainty in the closure test in data performed after integrating over the full p_T^{miss} range. The results, shown to the right of the solid line in Fig. 6, correspond to an uncertainty of 3% and 6% in the 3b and 4b bins, respectively.

7.2 Dilepton Z+jets control sample

As shown in Table 1, the second-largest background is Z+jets, with the Z boson decaying via $Z \rightarrow \nu\bar{\nu}$. Similarly to the $t\bar{t}$ case, we can validate the background estimation method for Z+jets events by constructing a closure test in a representative data control sample rich in $Z \rightarrow \ell^+\ell^-$

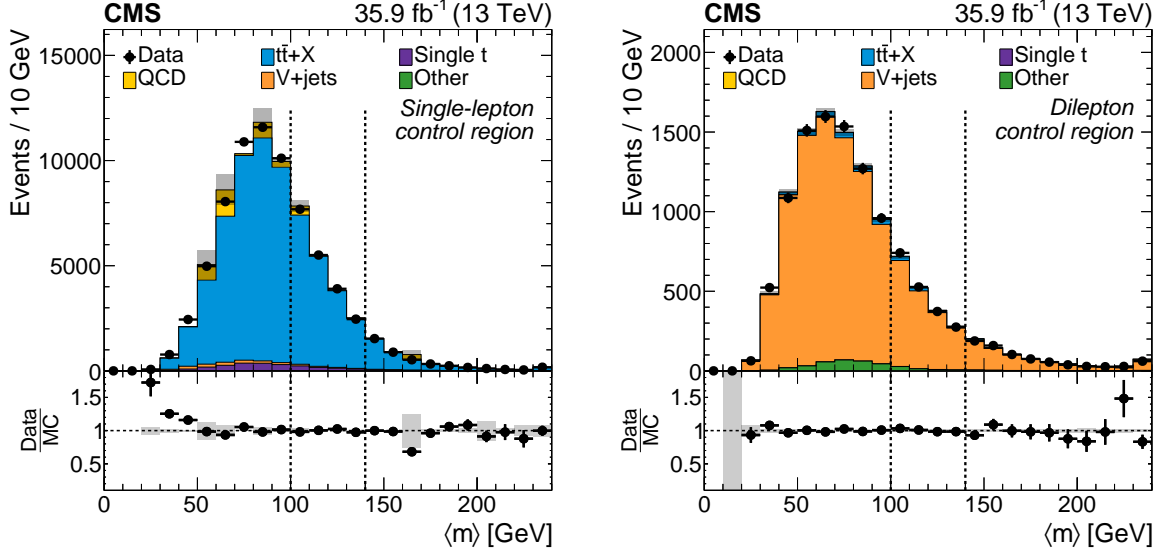


Figure 5: Comparison of the distributions of $\langle m \rangle$ in data and simulation in the single-lepton control sample (left) and in the dilepton control sample (right), where in both cases we have integrated over p_T^{miss} and b tag categories. The overall yields in simulation have been normalized to those observed in data. The gray shading indicates the statistical uncertainty in the total simulated background. The last bin includes overflow.

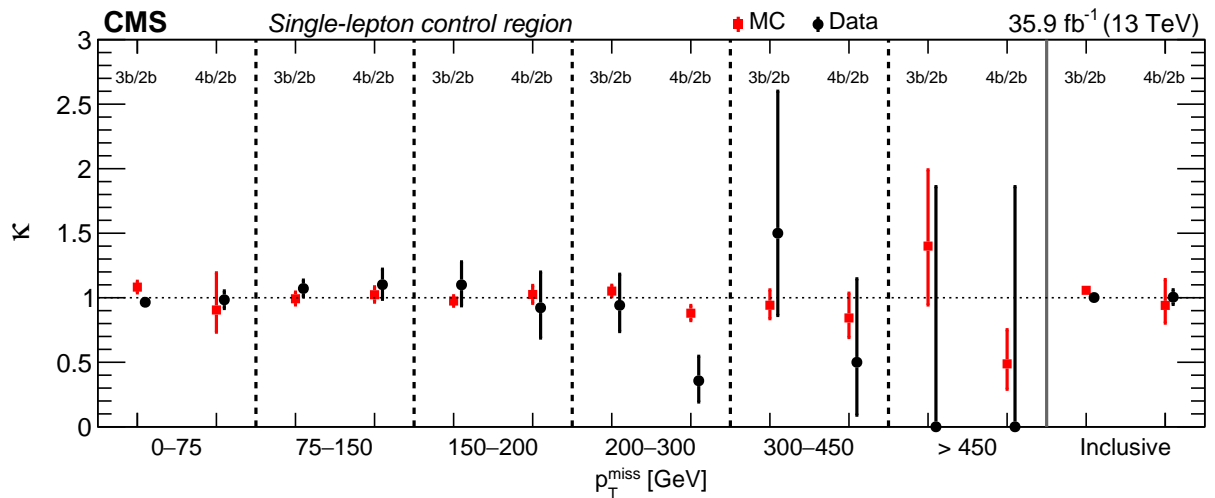


Figure 6: Comparison of the κ values found in the single-lepton control sample, for data and simulated events, for the 3b/2b and 4b/2b ABCD tests in each p_T^{miss} bin as well as after integrating over p_T^{miss} (labeled as “Inclusive”).

decays. However, given the small branching fraction of $Z \rightarrow \ell^+\ell^-$ decays and the large $t\bar{t}$ contamination associated with a high- N_b selection, we validate the method by constructing ABCD tests at lower b tag requirements, namely 1b/0b and 2b/1b.

The $Z \rightarrow \ell^+\ell^-$ control sample is constructed in a similar manner to the search region. Events with 4 or 5 jets are selected, and the reconstruction of a pair of Higgs bosons proceeds as described in Section 4. We require two opposite-charge same-flavor signal leptons in the Z boson mass window, $80 < m(\ell^+\ell^-) \leq 100$ GeV, with the p_T of the leading and subleading lepton required to be greater than 40 and 20 GeV, respectively. We remove the lepton and isolated track vetoes and, since the dilepton selection makes the contamination from QCD multijet events negligible, we remove the $\Delta\phi$ requirement. Since we do not expect genuine p_T^{miss} in $Z \rightarrow \ell^+\ell^-$ events, we additionally require $p_T^{\text{miss}} < 50$ GeV, which reduces the contamination from other processes from 20% to 10%.

We divide the sample in bins of $p_T(\ell^+\ell^-)$, ensuring kinematic correspondence with the $Z \rightarrow \nu\bar{\nu}$ decays present in the various p_T^{miss} bins employed in the search region. Similarly to the single-lepton sample, the presence of leptons allows us to extend the closure test to lower values of $p_T(\ell^+\ell^-)$. Figure 5 (right) shows both the high purity of the sample and the excellent data-to-simulation agreement in the $\langle m \rangle$ shape.

The validity of the extrapolation of the method to a sample consisting of lower b tag multiplicities is supported by the observation that all jets in Z +jets events come from ISR, and thus their kinematic properties are largely independent of the flavor content of the event. This expectation is confirmed in data by examining the overall closure of the method in bins of $p_T(\ell^+\ell^-)$ for the 1b/0b and 2b/1b ABCD tests. The 1b/0b test, which has greater statistical power compared to the 2b/1b test and thus allows a better examination of any potential trends as a function of $p_T(\ell^+\ell^-)$, is shown in Fig. 7 for illustration.

Since we do not observe that the closure of the method has any dependence on $p_T(\ell^+\ell^-)$, we proceed to combine all the $p_T(\ell^+\ell^-)$ bins into one bin and repeat the closure test with improved statistical precision. In the 1b/0b ABCD test, we observe a statistically significant nonclosure of 11%, which may be due to higher order effects beyond the precision of this search. The 2b/1b ABCD test shows good closure but with a higher statistical uncertainty of 19%. We assign the larger uncertainty of 19% as the systematic uncertainty in the closure of the background estimate method for Z +jets events. The robustness of this result is further corroborated by similar checks in a more inclusive selection without the ΔR_{max} requirement.

7.3 Low $\Delta\phi$ QCD multijet control sample

Finally, to examine the validity of the ABCD method for QCD multijet events, we define a control region enriched with such events by inverting the $\Delta\phi$ requirement. The high b tag multiplicity region of this control sample has a limited event yield and high $t\bar{t}$ contamination. To overcome these limitations, we exploit the fact that QCD multijet events, like Z +jets events, have similar kinematic properties regardless of their flavor content. We thus check the $\langle m \rangle$ - N_b independence in lower b tag multiplicity regions by constructing the 1b/0b and 2b/1b ABCD tests. We observe good agreement between the data and the simulation for all p_T^{miss} bins. The maximum measured deviation of κ from unity in the inclusive bins equals 13%, which we assign as the systematic uncertainty in the closure of the background estimation method for QCD multijet events.

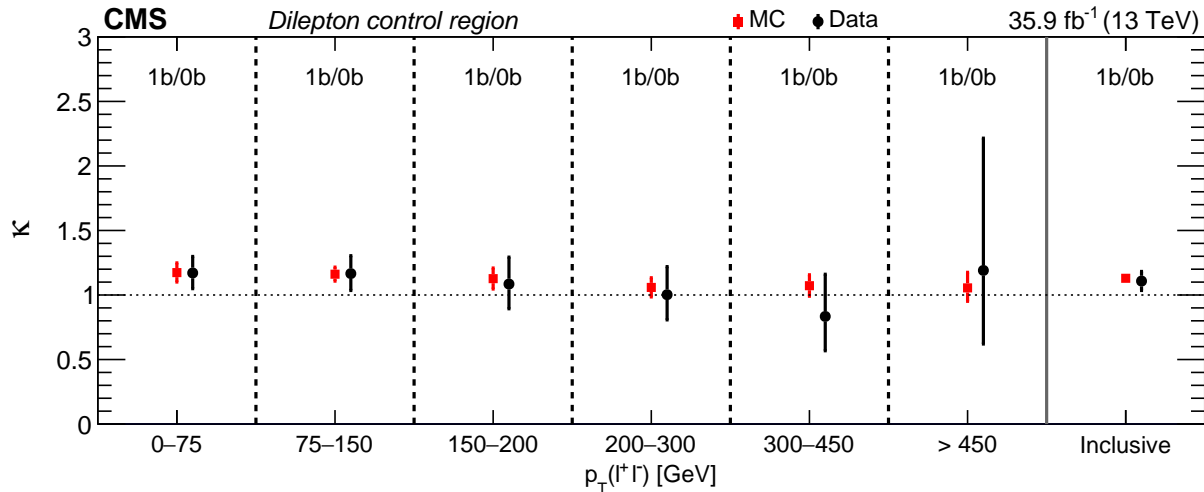


Figure 7: Comparison of the κ values found in the dilepton control sample, data and simulation, for the 1b/0b ABCD tests in bins of $p_T(\ell^+\ell^-)$ as well as after integrating over $p_T(\ell^+\ell^-)$ (labeled as “Inclusive”).

7.4 Impact of the background composition

Having evaluated the closure of the method for each individual background, we proceed to study the impact of mismodeling the relative abundance of the different background sources.

Since the $\langle m \rangle$ shape varies among background types, as shown for $t\bar{t}$ and Z+jets in Fig. 5, significant differences in the process admixture in the 2b category with respect to the 3b or 4b category will result in $\langle m \rangle$ - N_b correlation and lead to the nonclosure of the method. From simulation, the background composition is expected to be independent of the b tag category. The validity of this prediction relies on the ability of the simulation to model the shape of the b tag category and p_T^{miss} distributions equally well for each background contribution.

From comparisons in the respective control samples, we indeed observe that the N_b distribution for each of $t\bar{t}$, Z+jets, and QCD multijet production is similarly well modeled by the simulation. The p_T^{miss} distribution in simulation is found to overestimate the data for large values of p_T^{miss} for $t\bar{t}$ and Z+jets events, while the opposite is observed for QCD multijet events. To provide an estimate of the impact of mismodeling the background composition, we reweight the simulation based on the data-to-simulation comparisons and then calculate the κ factors with the reweighted simulation, assigning 100% of the shift with respect to the nominal values as the uncertainty in the modeling of the background composition. The resulting uncertainty is found to be at most 4%.

7.5 Total systematic uncertainty determination

Based on the data control sample studies described in Sections 7.1–7.4, we assign a set of systematic uncertainties in the background prediction for each search bin as follows:

1. The closure uncertainty for each background process obtained in data control regions is propagated to the background predictions by varying the closure of the particular background in simulation in bins of p_T^{miss} and N_b . The resulting shifts on the predictions, ranging from 1% to 10% increasing with p_T^{miss} , are assigned as systematic uncertainties with a 100% bin-to-bin correlation.
2. The level of nonclosure due to the relative abundance of each background component

as a function of N_b is estimated by comparing the change in κ in simulation before and after correcting the N_b and p_T^{miss} distributions of each background source according to measurements in the data control samples. Its overall impact is 1–4% and it is taken as 100% correlated across the different analysis bins.

3. The closure studies in the data control samples with more inclusive selections show no evidence of p_T^{miss} dependence, but have insufficient statistical power at high p_T^{miss} using the default selection. Given this limitation and the extensive validation of the simulation in all control samples, we assign the larger of the statistical uncertainty and the nonclosure for each bin in the simulation as the systematic uncertainty in the background prediction as a function of p_T^{miss} and N_b . As seen in Fig. 4, this uncertainty ranges from 8–15% in the lowest p_T^{miss} bin to 59–75% in the highest p_T^{miss} bin, and is assumed to be uncorrelated among bins.

Each of the listed uncertainties is incorporated in the background fit as a log-normal constraint in the likelihood function as described in Section 6.2, taking into account the stated correlations. Because of the robustness of the background prediction method, evidenced by the high-statistics data control region studies integrated in p_T^{miss} , the final uncertainty is dominated by the statistical precision of the simulation in evaluating the closure as a function of p_T^{miss} , described in the third item.

8 Results and interpretation

The observed event yields in data and the total predicted SM background are listed in Table 2, along with the expected yields for three higgsino mass scenarios. Two background estimates are given: the predictive fit, which does not use the data in the signal regions and ignores signal contamination in the other regions, and the global fit with $r = 0$, which incorporates the observations in the (HIG, 3b) and (HIG, 4b) regions, as described in Section 6.2. Since for $p_T^{\text{miss}} > 450 \text{ GeV}$ we observe no events in the (SBD, 4b) region, the parameter $\mu_{4b,\text{SBD}}^{\text{bkg}}$ is fitted to be zero, pushing against its physical boundary and leading to the underestimation of the associated uncertainty. We account for this by including an additional contribution that makes the uncertainty on $\mu_{4b,\text{SBD}}^{\text{bkg}}$ for $p_T^{\text{miss}} > 450 \text{ GeV}$ consistent with having observed one event. The event yields observed in data are consistent with the background predictions for all the analysis bins and no pattern of deviations is evident.

Figure 8 shows the distributions in data of $\langle m \rangle$ in the 3b and 4b bins for $150 < p_T^{\text{miss}} \leq 200 \text{ GeV}$ and $p_T^{\text{miss}} > 200 \text{ GeV}$. In each plot, the $\langle m \rangle$ histogram corresponding to the 2b category is normalized to the integral of the overlaid high- N_b category distribution. The shapes of the $\langle m \rangle$ distributions are consistent and no significant excess is observed in either the 3b or the 4b HIG regions.

The absence of excess event yields in data is interpreted in the context of the higgsino simplified model discussed in Section 1. Table 3 shows typical values for the systematic uncertainties associated with the expected signal yields for three models with different higgsino masses. The ranges correspond to the full variation of the uncertainties across all search bins. The uncertainty due to the pileup modeling is given by the difference between the signal efficiencies evaluated in samples with the mean number of reconstructed vertices found in the simulation and in the data, with the latter efficiencies obtained by extrapolation. The evaluation of the pileup uncertainty for very low higgsino masses is limited by the statistical power of the simulated samples. The remaining uncertainties are determined by comparing the nominal signal

Table 2: Event yields for all control regions—(HIG, 2b), (SBD, 2b), (SBD, 3b), and (SBD, 4b)—and the two signal regions—(HIG, 3b) and (HIG, 4b)—in each of the four p_T^{miss} bins. The second column shows the background yields predicted by the global fit which uses the observed yields in all control and signal regions, under the background-only hypothesis ($r = 0$). The third column gives the predicted SM background rates in the signal regions obtained via the predictive fit which only takes as input the observed event yields in the control regions. The expected signal yields for three signal benchmark points denoted as TChiHH($m_{\tilde{\chi}_1^0}, m_{\tilde{G}}$), with $m_{\tilde{\chi}_1^0}$ and $m_{\tilde{G}}$ in units of GeV, are also shown for reference.

Search region	Global fit	Predictive fit	Observed yields	TChiHH (225,1)	TChiHH (400,1)	TChiHH (700,1)
$150 < p_T^{\text{miss}} \leq 200 \text{ GeV}$						
SBD, 2b	$1560.1^{+39.7}_{-38.5}$	—	1559	5.8	1.3	0.0
HIG, 2b	$656.2^{+25.2}_{-24.6}$	—	658	11.5	2.4	0.1
SBD, 3b	$140.3^{+10.8}_{-10.3}$	—	145	5.1	0.9	0.0
HIG, 3b	$57.7^{+5.5}_{-5.2}$	$61.2^{+8.4}_{-7.7}$	53	10.9	2.5	0.1
SBD, 4b	$48.1^{+6.4}_{-5.8}$	—	45	5.8	1.1	0.0
HIG, 4b	$21.9^{+3.5}_{-3.2}$	$19.0^{+4.6}_{-3.9}$	25	21.8	5.4	0.2
$200 < p_T^{\text{miss}} \leq 300 \text{ GeV}$						
SBD, 2b	$588.0^{+24.2}_{-23.5}$	—	585	3.0	3.2	0.1
HIG, 2b	$333.1^{+17.9}_{-17.6}$	—	336	6.0	6.6	0.3
SBD, 3b	$55.3^{+6.5}_{-5.9}$	—	61	2.2	2.6	0.1
HIG, 3b	$30.6^{+3.9}_{-3.6}$	$35.1^{+5.9}_{-5.5}$	25	5.0	6.2	0.3
SBD, 4b	$15.6^{+3.8}_{-3.1}$	—	13	2.4	3.3	0.1
HIG, 4b	$11.4^{+3.0}_{-2.5}$	$7.5^{+3.8}_{-2.7}$	14	14.3	15.7	0.8
$300 < p_T^{\text{miss}} \leq 450 \text{ GeV}$						
SBD, 2b	$72.4^{+8.7}_{-8.1}$	—	74	0.0	1.9	0.2
HIG, 2b	$40.6^{+6.3}_{-6.0}$	—	39	0.4	4.9	0.7
SBD, 3b	$5.7^{+2.2}_{-1.8}$	—	4	0.1	1.6	0.2
HIG, 3b	$3.3^{+1.4}_{-1.1}$	$2.1^{+1.4}_{-1.0}$	5	0.9	4.6	0.5
SBD, 4b	$1.9^{+1.4}_{-0.9}$	—	2	0.2	1.5	0.2
HIG, 4b	$1.1^{+0.8}_{-0.5}$	$1.1^{+1.0}_{-0.6}$	1	2.0	10.3	1.5
$p_T^{\text{miss}} > 450 \text{ GeV}$						
SBD, 2b	$5.4^{+2.5}_{-2.1}$	—	5	0.0	0.1	0.2
HIG, 2b	$4.6^{+2.2}_{-1.9}$	—	5	0.0	0.4	0.9
SBD, 3b	$0.6^{+0.8}_{-0.4}$	—	1	0.1	0.1	0.2
HIG, 3b	$0.4^{+0.6}_{-0.3}$	$1.0^{+1.6}_{-1.0}$	0	0.0	0.4	0.7
SBD, 4b	$0.0^{+0.3}_{-0.0}$	—	0	0.0	0.1	0.2
HIG, 4b	$0.0^{+0.3}_{-0.0}$	$0.0^{+1.2}_{-0.0}$	0	0.0	1.1	2.0

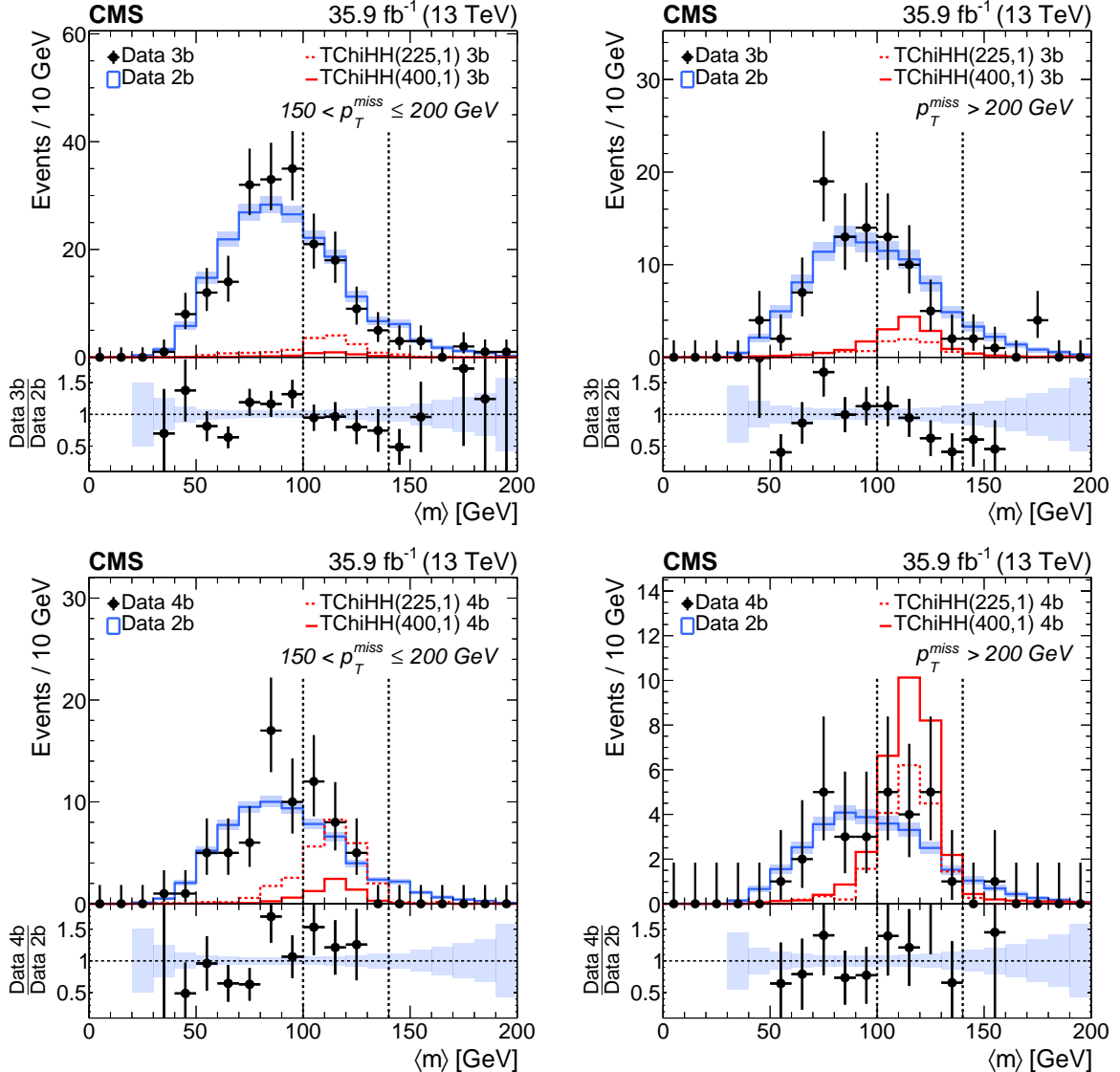


Figure 8: Distributions of $\langle m \rangle$ in data and two signal benchmark models denoted as $T\text{ChiHH}(m_{\tilde{\chi}_1^0}, m_{\tilde{G}})$, with $m_{\tilde{\chi}_1^0}$ and $m_{\tilde{G}}$ in units of GeV. The points with error bars show the data in the 3b (top) and 4b bins (bottom) for $150 < p_T^{\text{miss}} \leq 200 \text{ GeV}$ (left) and $p_T^{\text{miss}} > 200 \text{ GeV}$ (right). The histograms show the shapes of the $\langle m \rangle$ distributions observed in the 2b bins with overall event yields normalized to those observed in the 3b and 4b samples. The shaded areas reflect the statistical uncertainty in the $\langle m \rangle$ distribution in the 2b data. The vertical dashed lines denote the boundaries between the HIG and the SBD regions. The ratio plots demonstrate that the shapes are in agreement.

Table 3: Range of values for the systematic uncertainties in the signal efficiency and acceptance across the (HIG, 3b) and (HIG, 4b) bins for three signal benchmark points denoted as TChiHH($m_{\tilde{\chi}_1^0}, m_{\tilde{G}}$), with $m_{\tilde{\chi}_1^0}$ and $m_{\tilde{G}}$ in units of GeV. Uncertainties due to a particular source are treated as fully correlated among bins, while uncertainties due to different sources are treated as uncorrelated.

Source	Relative uncertainty [%]		
	TChiHH(225,1)	TChiHH(400,1)	TChiHH(700,1)
Trigger efficiency	1–6	1–6	1–6
b tagging efficiency	1–5	1–5	2–5
Fast sim. b tagging efficiency	2–10	4–8	3–13
Fast sim. p_T^{miss} resolution	14–27	1–6	1–7
Jet energy corrections	8–32	4–22	2–12
Jet energy resolution	3–23	1–18	1–11
Initial-state radiation	1–2	1	1
Jet identification	1	1	1
Pileup	1–31	1–6	1–5
Integrated luminosity	3	3	3

yield for each search region to the corresponding yield obtained after varying the scale factor or correction under study within its uncertainty. In the case of the ISR uncertainty, the variation is based on the full size of the ISR correction derived by comparing the transverse momentum of the jet system balancing the Z boson in $Z \rightarrow \ell^+ \ell^-$ events in data and in simulation. The largest uncertainties arise from the jet energy corrections, jet energy resolution, pileup modeling, and the p_T^{miss} resolution in the fast simulation. These uncertainties can be as large as 30% for low higgsino masses, but their impact is smaller for larger values of the higgsino mass. Uncertainties associated with the modeling of the b tagging range from 1% to 13%. The uncertainties in the trigger efficiency range from 6% in the lowest p_T^{miss} bin to <1% for $p_T^{\text{miss}} > 300$ GeV. Uncertainties due to the modeling of ISR and the efficiency of the jet identification filter are 1–2%. Finally, the systematic uncertainty in the total integrated luminosity is 2.5% [88].

The 95% confidence level (CL) upper limit on the production cross section for a pair of higgsinos in the context of the TChiHH simplified model is estimated using the modified frequentist CL_S method [89–91], with a one-sided profile likelihood ratio test statistic in its asymptotic approximation [92]. Figure 9 shows the expected and observed exclusion limits. The theoretical cross section at NLO+NLL [45, 46] as a function of higgsino mass is shown as a solid red line and the corresponding uncertainty as a dotted red line. The upper limits on the cross section at 95% CL for each mass point are obtained from the global fit method, which takes into account the expected signal contribution in all of the bins. Higgsinos with masses between 230 and 770 GeV are excluded.

The sensitivity at low higgsino mass is limited by the acceptance of the p_T^{miss} triggers employed in this analysis. As a result, final states corresponding to other Higgs boson decays that can be triggered independently of p_T^{miss} , such as $H \rightarrow \gamma\gamma$ [93] or $H \rightarrow WW$ [94], become more important in the low-mass region. For high higgsino mass, most of the signal events contribute to the highest p_T^{miss} bin, which has a negligible amount of background, so the sensitivity is mainly limited by the cross section for higgsino pair production.

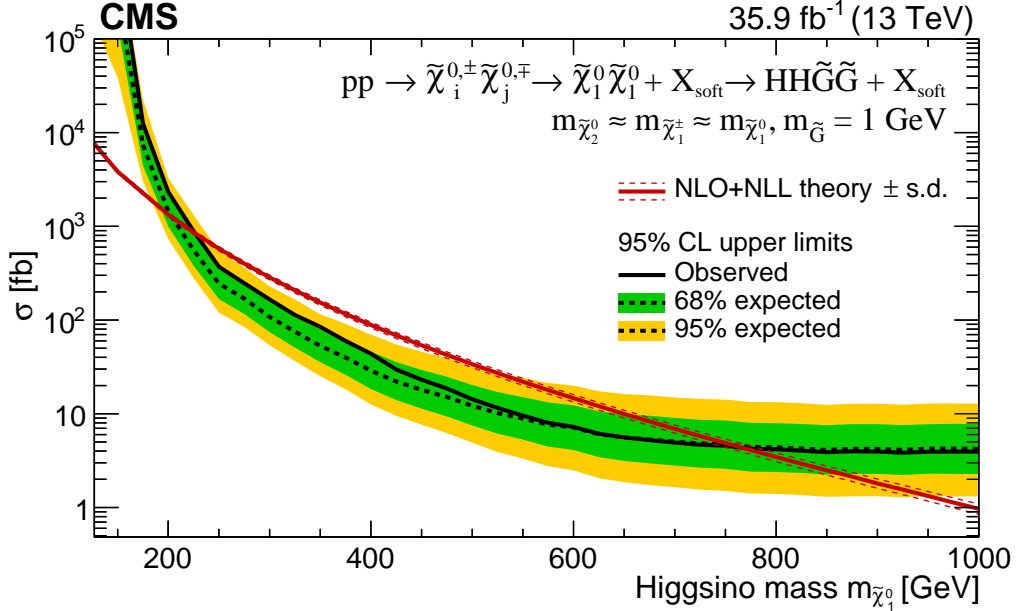


Figure 9: Expected (dashed black line) and observed (solid black line) excluded cross sections at 95% CL as a function of the higgsino mass. The theoretical cross section for the TChiHH simplified model is shown as the red solid line.

9 Summary

A search for an excess of events is performed in proton-proton collisions in the channel with two Higgs bosons and large missing transverse momentum (p_T^{miss}), with each of the Higgs bosons reconstructed in its $H \rightarrow b\bar{b}$ decay. The data sample corresponds to an integrated luminosity of 35.9 fb^{-1} at $\sqrt{s} = 13 \text{ TeV}$. Because the signal has four b quarks, while the background is dominated by $t\bar{t}$ events containing only two b quarks from the t quark decays, the analysis is binned in the number of b-tagged jets. In each event, the mass difference between the two Higgs boson candidates is required to be small, and the average mass of the two candidates is used in conjunction with the number of observed b tags to define signal and sideband regions. The observed event yields in these regions are used to obtain estimates for the standard model background in the signal regions without input from simulated event samples. The data are also binned in regions of p_T^{miss} to enhance the sensitivity to the signal.

The observed event yields in the signal regions are consistent with the background predictions. These results are interpreted in the context of a model in which each higgsino decays into a Higgs boson and a nearly massless lightest supersymmetric particle (LSP), which is weakly interacting. Such a scenario occurs in gauge-mediated supersymmetry breaking models, in which the LSP is a goldstino. The cross section calculation assumes that the higgsino sector is mass degenerate and sums over the cross sections for the pair production of all relevant combinations of higgsinos, but all decays are assumed to be prompt. Higgsinos with masses in the range 230 to 770 GeV are excluded at 95% confidence level. These results constitute the most stringent exclusion limits on this model to date.

Acknowledgments

We congratulate our colleagues in the CERN accelerator departments for the excellent performance of the LHC and thank the technical and administrative staffs at CERN and at other

CMS institutes for their contributions to the success of the CMS effort. In addition, we gratefully acknowledge the computing centers and personnel of the Worldwide LHC Computing Grid for delivering so effectively the computing infrastructure essential to our analyses. Finally, we acknowledge the enduring support for the construction and operation of the LHC and the CMS detector provided by the following funding agencies: BMWFW and FWF (Austria); FNRS and FWO (Belgium); CNPq, CAPES, FAPERJ, and FAPESP (Brazil); MES (Bulgaria); CERN; CAS, MoST, and NSFC (China); COLCIENCIAS (Colombia); MSES and CSF (Croatia); RPF (Cyprus); SENESCYT (Ecuador); MoER, ERC IUT, and ERDF (Estonia); Academy of Finland, MEC, and HIP (Finland); CEA and CNRS/IN2P3 (France); BMBF, DFG, and HGF (Germany); GSRT (Greece); OTKA and NIH (Hungary); DAE and DST (India); IPM (Iran); SFI (Ireland); INFN (Italy); MSIP and NRF (Republic of Korea); LAS (Lithuania); MOE and UM (Malaysia); BUAP, CINVESTAV, CONACYT, LNS, SEP, and UASLP-FAI (Mexico); MBIE (New Zealand); PAEC (Pakistan); MSHE and NSC (Poland); FCT (Portugal); JINR (Dubna); MON, RosAtom, RAS, RFBR and RAEP (Russia); MESTD (Serbia); SEIDI, CPAN, PCTI and FEDER (Spain); Swiss Funding Agencies (Switzerland); MST (Taipei); ThEPCenter, IPST, STAR, and NSTDA (Thailand); TUBITAK and TAEK (Turkey); NASU and SFFR (Ukraine); STFC (United Kingdom); DOE and NSF (USA).

Individuals have received support from the Marie-Curie program and the European Research Council and Horizon 2020 Grant, contract No. 675440 (European Union); the Leventis Foundation; the A. P. Sloan Foundation; the Alexander von Humboldt Foundation; the Belgian Federal Science Policy Office; the Fonds pour la Formation à la Recherche dans l’Industrie et dans l’Agriculture (FRIA-Belgium); the Agentschap voor Innovatie door Wetenschap en Technologie (IWT-Belgium); the Ministry of Education, Youth and Sports (MEYS) of the Czech Republic; the Council of Science and Industrial Research, India; the HOMING PLUS program of the Foundation for Polish Science, cofinanced from European Union, Regional Development Fund, the Mobility Plus program of the Ministry of Science and Higher Education, the National Science Center (Poland), contracts Harmonia 2014/14/M/ST2/00428, Opus 2014/13/B/ST2/02543, 2014/15/B/ST2/03998, and 2015/19/B/ST2/02861, Sonata-bis 2012/07/E/ST2/01406; the National Priorities Research Program by Qatar National Research Fund; the Programa Clarín-COFUND del Principado de Asturias; the Thalis and Aristeia programs cofinanced by EU-ESF and the Greek NSRF; the Rachadapisek Sompot Fund for Postdoctoral Fellowship, Chulalongkorn University and the Chulalongkorn Academic into Its 2nd Century Project Advancement Project (Thailand); the Welch Foundation, contract C-1845; and the Weston Havens Foundation (USA).

References

- [1] ATLAS Collaboration, “Observation of a new particle in the search for the Standard Model Higgs boson with the ATLAS detector at the LHC”, *Phys. Lett. B* **716** (2012) 1, doi:10.1016/j.physletb.2012.08.020, arXiv:1207.7214.
- [2] CMS Collaboration, “Observation of a new boson at a mass of 125 GeV with the CMS experiment at the LHC”, *Phys. Lett. B* **716** (2012) 30, doi:10.1016/j.physletb.2012.08.021, arXiv:1207.7235.
- [3] CMS Collaboration, “Observation of a new boson with mass near 125 GeV in pp collisions at $\sqrt{s} = 7$ and 8 TeV”, *JHEP* **06** (2013) 081, doi:10.1007/JHEP06(2013)081, arXiv:1303.4571.

- [4] CMS Collaboration, “Precise determination of the mass of the Higgs boson and tests of compatibility of its couplings with the standard model predictions using proton collisions at 7 and 8 TeV”, *Eur. Phys. J. C* **75** (2015) 212, doi:10.1140/epjc/s10052-015-3351-7, arXiv:1412.8662.
- [5] ATLAS Collaboration, “Measurement of the Higgs boson mass from the $H \rightarrow \gamma\gamma$ and $H \rightarrow ZZ^* \rightarrow 4\ell$ channels with the ATLAS detector using 25 fb^{-1} of pp collision data”, *Phys. Rev. D* **90** (2014) 052004, doi:10.1103/PhysRevD.90.052004, arXiv:1406.3827.
- [6] ATLAS and CMS Collaborations, “Combined measurement of the Higgs boson mass in pp collisions at $\sqrt{s} = 7$ and 8 TeV with the ATLAS and CMS experiments”, *Phys. Rev. Lett.* **114** (2015) 191803, doi:10.1103/PhysRevLett.114.191803, arXiv:1503.07589.
- [7] P. Ramond, “Dual theory for free fermions”, *Phys. Rev. D* **3** (1971) 2415, doi:10.1103/PhysRevD.3.2415.
- [8] Y. A. Gol’fand and E. P. Likhtman, “Extension of the algebra of Poincaré group generators and violation of P invariance”, *JETP Lett.* **13** (1971) 323.
- [9] A. Neveu and J. H. Schwarz, “Factorizable dual model of pions”, *Nucl. Phys. B* **31** (1971) 86, doi:10.1016/0550-3213(71)90448-2.
- [10] D. V. Volkov and V. P. Akulov, “Possible universal neutrino interaction”, *JETP Lett.* **16** (1972) 438.
- [11] J. Wess and B. Zumino, “A lagrangian model invariant under supergauge transformations”, *Phys. Lett. B* **49** (1974) 52, doi:10.1016/0370-2693(74)90578-4.
- [12] J. Wess and B. Zumino, “Supergauge transformations in four dimensions”, *Nucl. Phys. B* **70** (1974) 39, doi:10.1016/0550-3213(74)90355-1.
- [13] P. Fayet, “Supergauge invariant extension of the Higgs mechanism and a model for the electron and its neutrino”, *Nucl. Phys. B* **90** (1975) 104, doi:10.1016/0550-3213(75)90636-7.
- [14] H. P. Nilles, “Supersymmetry, supergravity and particle physics”, *Phys. Rep.* **110** (1984) 1, doi:10.1016/0370-1573(84)90008-5.
- [15] CMS Collaboration, “Searches for electroweak neutralino and chargino production in channels with Higgs, Z, and W bosons in pp collisions at 8 TeV”, *Phys. Rev. D* **90** (2014) 092007, doi:10.1103/PhysRevD.90.092007, arXiv:1409.3168.
- [16] CMS Collaboration, “Searches for electroweak production of charginos, neutralinos, and sleptons decaying to leptons and W, Z, and Higgs bosons in pp collisions at 8 TeV”, *Eur. Phys. J. C* **74** (2014) 3036, doi:10.1140/epjc/s10052-014-3036-7, arXiv:1405.7570.
- [17] CMS Collaboration, “Search for top squark and higgsino production using diphoton Higgs boson decays”, *Phys. Rev. Lett.* **112** (2014) 161802, doi:10.1103/PhysRevLett.112.161802, arXiv:1312.3310.

- [18] CMS Collaboration, “Search for top-squark pairs decaying into Higgs or Z bosons in pp collisions at $\sqrt{s} = 8$ TeV”, *Phys. Lett. B* **736** (2014) 371, doi:10.1016/j.physletb.2014.07.053, arXiv:1405.3886.
- [19] ATLAS Collaboration, “Search for direct pair production of a chargino and a neutralino decaying to the 125 GeV Higgs boson in $\sqrt{s} = 8$ TeV pp collisions with the ATLAS detector”, *Eur. Phys. J. C* **75** (2015) 208, doi:10.1140/epjc/s10052-015-3408-7, arXiv:1501.07110.
- [20] ATLAS Collaboration, “Search for supersymmetry in events with photons, bottom quarks, and missing transverse momentum in proton-proton collisions at a centre-of-mass energy of 7 TeV with the ATLAS detector”, *Phys. Lett. B* **719** (2013) 261, doi:10.1016/j.physletb.2013.01.041, arXiv:1211.1167.
- [21] G. ’t Hooft, “Naturalness, chiral symmetry, and spontaneous chiral symmetry breaking”, *NATO Sci. Ser. B* **59** (1980) 135, doi:10.1007/978-1-4684-7571-5_9.
- [22] E. Witten, “Dynamical breaking of supersymmetry”, *Nucl. Phys. B* **188** (1981) 513, doi:10.1016/0550-3213(81)90006-7.
- [23] M. Dine, W. Fischler, and M. Srednicki, “Supersymmetric technicolor”, *Nucl. Phys. B* **189** (1981) 575, doi:10.1016/0550-3213(81)90582-4.
- [24] S. Dimopoulos and S. Raby, “Supercolor”, *Nucl. Phys. B* **192** (1981) 353, doi:10.1016/0550-3213(81)90430-2.
- [25] S. Dimopoulos and H. Georgi, “Softly broken supersymmetry and SU(5)”, *Nucl. Phys. B* **193** (1981) 150, doi:10.1016/0550-3213(81)90522-8.
- [26] R. K. Kaul and P. Majumdar, “Cancellation of quadratically divergent mass corrections in globally supersymmetric spontaneously broken gauge theories”, *Nucl. Phys. B* **199** (1982) 36, doi:10.1016/0550-3213(82)90565-X.
- [27] R. Barbieri and G. F. Giudice, “Upper bounds on supersymmetric particle masses”, *Nucl. Phys. B* **306** (1988) 63, doi:10.1016/0550-3213(88)90171-X.
- [28] S. Dimopoulos and G. F. Giudice, “Naturalness constraints in supersymmetric theories with nonuniversal soft terms”, *Phys. Lett. B* **357** (1995) 573, doi:10.1016/0370-2693(95)00961-J, arXiv:hep-ph/9507282.
- [29] R. Barbieri and D. Pappadopulo, “S-particles at their naturalness limits”, *JHEP* **10** (2009) 061, doi:10.1088/1126-6708/2009/10/061, arXiv:0906.4546.
- [30] M. Papucci, J. T. Ruderman, and A. Weiler, “Natural SUSY endures”, *JHEP* **09** (2012) 035, doi:10.1007/JHEP09(2012)035, arXiv:1110.6926.
- [31] J. L. Feng, “Naturalness and the Status of Supersymmetry”, *Ann. Rev. Nucl. Part. Sci.* **63** (2013) 351, doi:10.1146/annurev-nucl-102010-130447, arXiv:1302.6587.
- [32] G. R. Farrar and P. Fayet, “Phenomenology of the production, decay, and detection of new hadronic states associated with supersymmetry”, *Phys. Lett. B* **76** (1978) 575, doi:10.1016/0370-2693(78)90858-4.
- [33] Z. Han, G. D. Kribs, A. Martin, and A. Menon, “Hunting quasidegenerate Higgsinos”, *Phys. Rev. D* **89** (2014) 075007, doi:10.1103/PhysRevD.89.075007, arXiv:1401.1235.

- [34] C. Han, D. Kim, S. Munir, and M. Park, “Accessing the core of naturalness, nearly degenerate higgsinos, at the LHC”, *JHEP* **04** (2015) 132, doi:10.1007/JHEP04(2015)132, arXiv:1502.03734.
- [35] H. Baer et al., “Physics at a Higgsino factory”, *JHEP* **06** (2014) 172, doi:10.1007/JHEP06(2014)172, arXiv:1404.7510.
- [36] ATLAS Collaboration, “Search for new phenomena in final states with an energetic jet and large missing transverse momentum in pp collisions at $\sqrt{s} = 8$ TeV with the ATLAS detector”, *Eur. Phys. J. C* **75** (2015) 299, doi:10.1140/epjc/s10052-015-3517-3, arXiv:1502.01518. [Erratum: doi:10.1140/epjc/s10052-015-3639-7].
- [37] CMS Collaboration, “Search for dark matter in proton-proton collisions at 8 TeV with missing transverse momentum and vector boson tagged jets”, *JHEP* **12** (2016) 083, doi:10.1007/JHEP12(2016)083, arXiv:1607.05764.
- [38] ATLAS Collaboration, “Search for new phenomena in final states with an energetic jet and large missing transverse momentum in pp collisions at $\sqrt{s} = 13$ TeV using the ATLAS detector”, *Phys. Rev. D* **94** (2016) 032005, doi:10.1103/PhysRevD.94.032005, arXiv:1604.07773.
- [39] ATLAS Collaboration, “Search for dark matter produced in association with a hadronically decaying vector boson in pp collisions at $\sqrt{s} = 13$ TeV with the ATLAS detector”, *Phys. Lett. B* **763** (2016) 251, doi:10.1016/j.physletb.2016.10.042, arXiv:1608.02372.
- [40] CMS Collaboration, “Search for dark matter produced with an energetic jet or a hadronically decaying W or Z boson at $\sqrt{s} = 13$ TeV”, *JHEP* **07** (2017) doi:10.1007/JHEP07(2017)014, arXiv:1703.01651. Submitted to *JHEP*.
- [41] C. Han et al., “Probing light Higgsinos in natural SUSY from monojet signals at the LHC”, *JHEP* **02** (2014) 049, doi:10.1007/JHEP02(2014)049, arXiv:1310.4274.
- [42] J. T. Ruderman and D. Shih, “General Neutralino NLSPs at the Early LHC”, *JHEP* **08** (2012) 159, doi:10.1007/JHEP08(2012)159, arXiv:1103.6083.
- [43] S. Dimopoulos, M. Dine, S. Raby, and S. D. Thomas, “Experimental signatures of low-energy gauge mediated supersymmetry breaking”, *Phys. Rev. Lett.* **76** (1996) 3494, doi:10.1103/PhysRevLett.76.3494, arXiv:hep-ph/9601367.
- [44] K. T. Matchev and S. D. Thomas, “Higgs and Z boson signatures of supersymmetry”, *Phys. Rev. D* **62** (2000) 077702, doi:10.1103/PhysRevD.62.077702, arXiv:hep-ph/9908482.
- [45] B. Fuks, M. Klasen, D. R. Lamprea, and M. Rothering, “Gaugino production in proton-proton collisions at a center-of-mass energy of 8 TeV”, *JHEP* **10** (2012) 081, doi:10.1007/JHEP10(2012)081, arXiv:1207.2159.
- [46] B. Fuks, M. Klasen, D. R. Lamprea, and M. Rothering, “Precision predictions for electroweak superpartner production at hadron colliders with RESUMMINO”, *Eur. Phys. J. C* **73** (2013) 2480, doi:10.1140/epjc/s10052-013-2480-0, arXiv:1304.0790.
- [47] J. Alwall, P. C. Schuster, and N. Toro, “Simplified models for a first characterization of new physics at the LHC”, *Phys. Rev. D* **79** (2009) 075020, doi:10.1103/PhysRevD.79.075020, arXiv:0810.3921.

- [48] J. Alwall, M.-P. Le, M. Lisanti, and J. G. Wacker, “Model-independent jets plus missing energy searches”, *Phys. Rev. D* **79** (2009) 015005, doi:10.1103/PhysRevD.79.015005, arXiv:0809.3264.
- [49] D. Alves et al., “Simplified models for LHC new physics searches”, *J. Phys. G* **39** (2012) 105005, doi:10.1088/0954-3899/39/10/105005, arXiv:1105.2838.
- [50] P. Meade, M. Reece, and D. Shih, “Prompt decays of general neutralino NLSPs at the Tevatron”, *JHEP* **05** (2010) 105, doi:10.1007/JHEP05(2010)105, arXiv:0911.4130.
- [51] CMS Collaboration, “The CMS experiment at the CERN LHC”, *JINST* **3** (2008) S08004, doi:10.1088/1748-0221/3/08/S08004.
- [52] J. Alwall et al., “The automated computation of tree-level and next-to-leading order differential cross sections, and their matching to parton shower simulations”, *JHEP* **07** (2014) 079, doi:10.1007/JHEP07(2014)079, arXiv:1405.0301.
- [53] J. Alwall et al., “Comparative study of various algorithms for the merging of parton showers and matrix elements in hadronic collisions”, *Eur. Phys. J. C* **53** (2008) 473, doi:10.1140/epjc/s10052-007-0490-5, arXiv:0706.2569.
- [54] S. Alioli, P. Nason, C. Oleari, and E. Re, “NLO single-top production matched with shower in POWHEG: s - and t -channel contributions”, *JHEP* **09** (2009) 111, doi:10.1088/1126-6708/2009/09/111, arXiv:0907.4076. [Erratum: doi:10.1007/JHEP02(2010)011].
- [55] E. Re, “Single-top Wt -channel production matched with parton showers using the POWHEG method”, *Eur. Phys. J. C* **71** (2011) 1547, doi:10.1140/epjc/s10052-011-1547-z, arXiv:1009.2450.
- [56] R. Frederix and S. Frixione, “Merging meets matching in MC@NLO”, *JHEP* **12** (2012) 061, doi:10.1007/JHEP12(2012)061, arXiv:1209.6215.
- [57] NNPDF Collaboration, “Parton distributions for the LHC Run II”, *JHEP* **04** (2015) 040, doi:10.1007/JHEP04(2015)040, arXiv:1410.8849.
- [58] T. Sjöstrand et al., “An introduction to PYTHIA 8.2”, *Comput. Phys. Commun.* **191** (2015) 159, doi:10.1016/j.cpc.2015.01.024, arXiv:1410.3012.
- [59] CMS Collaboration, “Event generator tunes obtained from underlying event and multiparton scattering measurements”, *Eur. Phys. J. C* **76** (2016) 155, doi:10.1140/epjc/s10052-016-3988-x, arXiv:1512.00815.
- [60] GEANT4 Collaboration, “GEANT4 — a simulation toolkit”, *Nucl. Instrum. Meth. A* **506** (2003) 250, doi:10.1016/S0168-9002(03)01368-8.
- [61] J. Allison et al., “GEANT4 developments and applications”, *IEEE Trans. Nucl. Sci.* **53** (2006) 270, doi:10.1109/TNS.2006.869826.
- [62] J. Allison et al., “Recent developments in GEANT4”, *Nucl. Instrum. Meth. A* **835** (2016) 186, doi:10.1016/j.nima.2016.06.125.
- [63] M. Beneke, P. Falgari, S. Klein, and C. Schwinn, “Hadronic top-quark pair production with NNLL threshold resummation”, *Nucl. Phys. B* **855** (2012) 695, doi:10.1016/j.nuclphysb.2011.10.021, arXiv:1109.1536.

- [64] M. Cacciari et al., “Top-pair production at hadron colliders with next-to-next-to-leading logarithmic soft-gluon resummation”, *Phys. Lett. B* **710** (2012) 612, doi:10.1016/j.physletb.2012.03.013, arXiv:1111.5869.
- [65] P. Bärnreuther, M. Czakon, and A. Mitov, “Percent-level-precision physics at the Tevatron: Next-to-next-to-leading order QCD corrections to $q\bar{q} \rightarrow t\bar{t} + X$ ”, *Phys. Rev. Lett.* **109** (2012) 132001, doi:10.1103/PhysRevLett.109.132001, arXiv:1204.5201.
- [66] M. Czakon and A. Mitov, “NNLO corrections to top-pair production at hadron colliders: the all-fermionic scattering channels”, *JHEP* **12** (2012) 054, doi:10.1007/JHEP12(2012)054, arXiv:1207.0236.
- [67] M. Czakon and A. Mitov, “NNLO corrections to top pair production at hadron colliders: the quark-gluon reaction”, *JHEP* **01** (2013) 080, doi:10.1007/JHEP01(2013)080, arXiv:1210.6832.
- [68] M. Czakon, P. Fiedler, and A. Mitov, “Total top-quark pair-production cross section at hadron colliders through $O(\alpha_S^4)$ ”, *Phys. Rev. Lett.* **110** (2013) 252004, doi:10.1103/PhysRevLett.110.252004, arXiv:1303.6254.
- [69] R. Gavin, Y. Li, F. Petriello, and S. Quackenbush, “W Physics at the LHC with FEWZ 2.1”, *Comput. Phys. Commun.* **184** (2013) 208, doi:10.1016/j.cpc.2012.09.005, arXiv:1201.5896.
- [70] R. Gavin, Y. Li, F. Petriello, and S. Quackenbush, “FEWZ 2.0: A code for hadronic Z production at next-to-next-to-leading order”, *Comput. Phys. Commun.* **182** (2011) 2388, doi:10.1016/j.cpc.2011.06.008, arXiv:1011.3540.
- [71] T. Melia, P. Nason, R. Rontsch, and G. Zanderighi, “W+W-, WZ and ZZ production in the POWHEG BOX”, *JHEP* **11** (2011) 078, doi:10.1007/JHEP11(2011)078, arXiv:1107.5051.
- [72] P. Z. Skands et al., “SUSY Les Houches accord: Interfacing SUSY spectrum calculators, decay packages, and event generators”, *JHEP* **07** (2004) 036, doi:10.1088/1126-6708/2004/07/036, arXiv:hep-ph/0311123.
- [73] D. de Florian et al., “Handbook of LHC Higgs cross sections: 4. deciphering the nature of the Higgs sector”, CERN Report CERN-2017-002-M, 2016. doi:10.23731/CYRM-2017-002, arXiv:1610.07922.
- [74] S. Abdullin et al., “The fast simulation of the CMS detector at LHC”, *J. Phys. Conf. Ser.* **331** (2011) 032049, doi:10.1088/1742-6596/331/3/032049.
- [75] CMS Collaboration, “Particle-flow reconstruction and global event description with the CMS detector”, (2017). arXiv:1706.04965. Submitted to JINST.
- [76] M. Cacciari, G. P. Salam, and G. Soyez, “The anti- k_t jet clustering algorithm”, *JHEP* **04** (2008) 063, doi:10.1088/1126-6708/2008/04/063, arXiv:0802.1189.
- [77] M. Cacciari, G. P. Salam, and G. Soyez, “FastJet user manual”, *Eur. Phys. J. C* **72** (2012) 1896, doi:10.1140/epjc/s10052-012-1896-2, arXiv:1111.6097.
- [78] CMS Collaboration, “Jet energy scale and resolution in the CMS experiment in pp collisions at 8 TeV”, *JINST* **12** (2017) P02014, doi:10.1088/1748-0221/12/02/P02014, arXiv:1607.03663.

- [79] CMS Collaboration, “Jet performance in pp collisions at $\sqrt{s} = 7$ TeV”, CMS Physics Analysis Summary CMS-PAS-JME-10-003, 2010.
- [80] CMS Collaboration, “Identification of heavy-flavour jets with the CMS detector in pp collisions at 13 TeV”, (2017). arXiv:1712.07158. Submitted to JINST.
- [81] D. Guest et al., “Jet flavor classification in high-energy physics with deep neural networks”, *Phys. Rev. D* **94** (2016) 112002, doi:10.1103/PhysRevD.94.112002, arXiv:1607.08633.
- [82] CMS Collaboration, “Particle flow event reconstruction in CMS and performance for jets, taus and E_T^{miss} ”, CMS Physics Analysis Summary CMS-PAS-PFT-09-001, 2009.
- [83] CMS Collaboration, “Commissioning of the particle-flow event reconstruction with the first lhc collisions recorded in the cms detector”, CMS Physics Analysis Summary CMS-PAS-PFT-10-001, 2010.
- [84] CMS Collaboration, “Performance of electron reconstruction and selection with the CMS detector in proton-proton collisions at $\sqrt{s} = 8$ TeV”, *JINST* **10** (2015) P06005, doi:10.1088/1748-0221/10/06/P06005, arXiv:1502.02701.
- [85] CMS Collaboration, “Performance of CMS muon reconstruction in pp collision events at $\sqrt{s} = 7$ TeV”, *JINST* **7** (2012) P10002, doi:10.1088/1748-0221/7/10/P10002, arXiv:1206.4071.
- [86] K. Rehermann and B. Tweedie, “Efficient identification of boosted semileptonic top quarks at the LHC”, *JHEP* **03** (2011) 059, doi:10.1007/JHEP03(2011)059, arXiv:1007.2221.
- [87] CMS Collaboration, “Search for supersymmetry in pp collisions at $\sqrt{s} = 13$ TeV in the single-lepton final state using the sum of masses of large-radius jets”, *JHEP* **08** (2016) 122, doi:10.1007/JHEP08(2016)122, arXiv:1605.04608.
- [88] CMS Collaboration, “CMS luminosity measurements for the 2016 data taking period”, CMS Physics Analysis Summary CMS-PAS-LUM-17-001, 2017.
- [89] T. Junk, “Confidence level computation for combining searches with small statistics”, *Nucl. Instrum. Meth. A* **434** (1999) 435, doi:10.1016/S0168-9002(99)00498-2, arXiv:hep-ex/9902006.
- [90] A. L. Read, “Presentation of search results: the CL_s technique”, in *Durham IPPP Workshop: Advanced Statistical Techniques in Particle Physics*, p. 2693. Durham, UK, March, 2002. [*J. Phys. G* **28** (2002) 2693]. doi:10.1088/0954-3899/28/10/313.
- [91] ATLAS Collaboration, CMS Collaboration, LHC Higgs Combination Group, “Procedure for the LHC Higgs boson search combination in Summer 2011”, Technical Report CMS-NOTE-2011-005, ATL-PHYS-PUB-2011-11, CERN, 2011.
- [92] G. Cowan, K. Cranmer, E. Gross, and O. Vitells, “Asymptotic formulae for likelihood-based tests of new physics”, *Eur. Phys. J. C* **71** (2011) 1554, doi:10.1140/epjc/s10052-011-1554-0, arXiv:1007.1727. [Erratum: doi:10.1140/epjc/s10052-013-2501-z].

- [93] CMS Collaboration, “Search for supersymmetry with Higgs boson to diphoton decays using the razor variables at $\sqrt{s} = 13$ TeV”, (2017). arXiv:1709.00384. Submitted to *Phys. Lett. B*.
- [94] CMS Collaboration, “Search for electroweak production of charginos and neutralinos in multilepton final states in proton-proton collisions at $\sqrt{s} = 13$ TeV”, arXiv:1709.05406. Submitted to *JHEP*.

A The CMS Collaboration

Yerevan Physics Institute, Yerevan, Armenia

A.M. Sirunyan, A. Tumasyan

Institut für Hochenergiephysik, Wien, Austria

W. Adam, F. Ambrogi, E. Asilar, T. Bergauer, J. Brandstetter, E. Brondolin, M. Dragicevic, J. Erö, M. Flechl, M. Friedl, R. Frühwirth¹, V.M. Ghete, J. Grossmann, J. Hrubec, M. Jeitler¹, A. König, N. Krammer, I. Krätschmer, D. Liko, T. Madlener, I. Mikulec, E. Pree, D. Rabady, N. Rad, H. Rohringer, J. Schieck¹, R. Schöfbeck, M. Spanring, D. Spitzbart, J. Strauss, W. Waltenberger, J. Wittmann, C.-E. Wulz¹, M. Zarucki

Institute for Nuclear Problems, Minsk, Belarus

V. Chekhovsky, V. Mossolov, J. Suarez Gonzalez

Universiteit Antwerpen, Antwerpen, Belgium

E.A. De Wolf, D. Di Croce, X. Janssen, J. Lauwers, M. Van De Klundert, H. Van Haevermaet, P. Van Mechelen, N. Van Remortel

Vrije Universiteit Brussel, Brussel, Belgium

S. Abu Zeid, F. Blekman, J. D'Hondt, I. De Bruyn, J. De Clercq, K. Deroover, G. Flouris, D. Lontkovskyi, S. Lowette, S. Moortgat, L. Moreels, A. Olbrechts, Q. Python, K. Skovpen, S. Tavernier, W. Van Doninck, P. Van Mulders, I. Van Parijs

Université Libre de Bruxelles, Bruxelles, Belgium

H. Brun, B. Clerbaux, G. De Lentdecker, H. Delannoy, G. Fasanella, L. Favart, R. Goldouzian, A. Grebenyuk, G. Karapostoli, T. Lenzi, J. Luetic, T. Maerschalk, A. Marinov, A. Randle-conde, T. Seva, C. Vander Velde, P. Vanlaer, D. Vannerom, R. Yonamine, F. Zenoni, F. Zhang²

Ghent University, Ghent, Belgium

A. Cimmino, T. Cornelis, D. Dobur, A. Fagot, M. Gul, I. Khvastunov, D. Poyraz, C. Roskas, S. Salva, M. Tytgat, W. Verbeke, N. Zaganidis

Université Catholique de Louvain, Louvain-la-Neuve, Belgium

H. Bakhshiansohi, O. Bondu, S. Brochet, G. Bruno, A. Caudron, S. De Visscher, C. Delaere, M. Delcourt, B. Francois, A. Giannanco, A. Jafari, M. Komm, G. Krintiras, V. Lemaitre, A. Magitteri, A. Mertens, M. Musich, K. Piotrkowski, L. Quertenmont, M. Vidal Marono, S. Wertz

Université de Mons, Mons, Belgium

N. Belyi

Centro Brasileiro de Pesquisas Fisicas, Rio de Janeiro, Brazil

W.L. Aldá Júnior, F.L. Alves, G.A. Alves, L. Brito, M. Correa Martins Junior, C. Hensel, A. Moraes, M.E. Pol, P. Rebello Teles

Universidade do Estado do Rio de Janeiro, Rio de Janeiro, Brazil

E. Belchior Batista Das Chagas, W. Carvalho, J. Chinellato³, A. Custódio, E.M. Da Costa, G.G. Da Silveira⁴, D. De Jesus Damiao, S. Fonseca De Souza, L.M. Huertas Guativa, H. Malbouisson, M. Melo De Almeida, C. Mora Herrera, L. Mundim, H. Nogima, A. Santoro, A. Sznajder, E.J. Tonelli Manganote³, F. Torres Da Silva De Araujo, A. Vilela Pereira

Universidade Estadual Paulista ^a, Universidade Federal do ABC ^b, São Paulo, Brazil

S. Ahuja^a, C.A. Bernardes^a, T.R. Fernandez Perez Tomei^a, E.M. Gregores^b, P.G. Mercadante^b, S.F. Novaes^a, Sandra S. Padula^a, D. Romero Abad^b, J.C. Ruiz Vargas^a

Institute for Nuclear Research and Nuclear Energy of Bulgaria Academy of Sciences

A. Aleksandrov, R. Hadjiiska, P. Iaydjiev, M. Misheva, M. Rodozov, M. Shopova, S. Stoykova, G. Sultanov

University of Sofia, Sofia, Bulgaria

A. Dimitrov, I. Glushkov, L. Litov, B. Pavlov, P. Petkov

Beihang University, Beijing, China

W. Fang⁵, X. Gao⁵

Institute of High Energy Physics, Beijing, China

M. Ahmad, J.G. Bian, G.M. Chen, H.S. Chen, M. Chen, Y. Chen, C.H. Jiang, D. Leggat, H. Liao, Z. Liu, F. Romeo, S.M. Shaheen, A. Spiezia, J. Tao, C. Wang, Z. Wang, E. Yazgan, H. Zhang, J. Zhao

State Key Laboratory of Nuclear Physics and Technology, Peking University, Beijing, China

Y. Ban, G. Chen, Q. Li, S. Liu, Y. Mao, S.J. Qian, D. Wang, Z. Xu

Universidad de Los Andes, Bogota, Colombia

C. Avila, A. Cabrera, L.F. Chaparro Sierra, C. Florez, C.F. González Hernández, J.D. Ruiz Alvarez

University of Split, Faculty of Electrical Engineering, Mechanical Engineering and Naval Architecture, Split, Croatia

B. Courbon, N. Godinovic, D. Lelas, I. Puljak, P.M. Ribeiro Cipriano, T. Sculac

University of Split, Faculty of Science, Split, Croatia

Z. Antunovic, M. Kovac

Institute Rudjer Boskovic, Zagreb, Croatia

V. Brigljevic, D. Ferencek, K. Kadija, B. Mesic, A. Starodumov⁶, T. Susa

University of Cyprus, Nicosia, Cyprus

M.W. Ather, A. Attikis, G. Mavromanolakis, J. Mousa, C. Nicolaou, F. Ptochos, P.A. Razis, H. Rykaczewski

Charles University, Prague, Czech Republic

M. Finger⁷, M. Finger Jr.⁷

Universidad San Francisco de Quito, Quito, Ecuador

E. Carrera Jarrin

Academy of Scientific Research and Technology of the Arab Republic of Egypt, Egyptian Network of High Energy Physics, Cairo, Egypt

Y. Assran^{8,9}, M.A. Mahmoud^{10,9}, A. Mahrouse¹¹

National Institute of Chemical Physics and Biophysics, Tallinn, Estonia

R.K. Dewanjee, M. Kadastik, L. Perrini, M. Raidal, A. Tiko, C. Veelken

Department of Physics, University of Helsinki, Helsinki, Finland

P. Eerola, J. Pekkanen, M. Voutilainen

Helsinki Institute of Physics, Helsinki, Finland

J. Häkkinen, T. Järvinen, V. Karimäki, R. Kinnunen, T. Lampén, K. Lassila-Perini, S. Lehti, T. Lindén, P. Luukka, E. Tuominen, J. Tuominiemi, E. Tuovinen

Lappeenranta University of Technology, Lappeenranta, Finland

J. Talvitie, T. Tuuva

IRFU, CEA, Université Paris-Saclay, Gif-sur-Yvette, France

M. Besancon, F. Couderc, M. Dejardin, D. Denegri, J.L. Faure, F. Ferri, S. Ganjour, S. Ghosh, A. Givernaud, P. Gras, G. Hamel de Monchenault, P. Jarry, I. Kucher, E. Locci, M. Machet, J. Malcles, G. Negro, J. Rander, A. Rosowsky, M.Ö. Sahin, M. Titov

Laboratoire Leprince-Ringuet, Ecole polytechnique, CNRS/IN2P3, Université Paris-Saclay, Palaiseau, France

A. Abdulsalam, I. Antropov, S. Baffioni, F. Beaudette, P. Busson, L. Cadamuro, C. Charlot, R. Granier de Cassagnac, M. Jo, S. Lisniak, A. Lobanov, J. Martin Blanco, M. Nguyen, C. Ochando, G. Ortona, P. Paganini, P. Pigard, S. Regnard, R. Salerno, J.B. Sauvan, Y. Sirois, A.G. Stahl Leiton, T. Strebler, Y. Yilmaz, A. Zabi, A. Zghiche

Université de Strasbourg, CNRS, IPHC UMR 7178, F-67000 Strasbourg, FranceJ.-L. Agram¹², J. Andrea, D. Bloch, J.-M. Brom, M. Buttignol, E.C. Chabert, N. Chanon, C. Collard, E. Conte¹², X. Coubez, J.-C. Fontaine¹², D. Gelé, U. Goerlach, M. Jansová, A.-C. Le Bihan, N. Tonon, P. Van Hove**Centre de Calcul de l’Institut National de Physique Nucléaire et de Physique des Particules, CNRS/IN2P3, Villeurbanne, France**

S. Gadrat

Université de Lyon, Université Claude Bernard Lyon 1, CNRS-IN2P3, Institut de Physique Nucléaire de Lyon, Villeurbanne, FranceS. Beauceron, C. Bernet, G. Boudoul, R. Chierici, D. Contardo, P. Depasse, H. El Mamouni, J. Fay, L. Finco, S. Gascon, M. Gouzevitch, G. Grenier, B. Ille, F. Lagarde, I.B. Laktineh, M. Lethuillier, L. Mirabito, A.L. Pequegnot, S. Perries, A. Popov¹³, V. Sordini, M. Vander Donckt, S. Viret**Georgian Technical University, Tbilisi, Georgia**A. Khvedelidze⁷**Tbilisi State University, Tbilisi, Georgia**I. Bagaturia¹⁴**RWTH Aachen University, I. Physikalisches Institut, Aachen, Germany**

C. Autermann, S. Beranek, L. Feld, M.K. Kiesel, K. Klein, M. Lipinski, M. Preuten, C. Schomakers, J. Schulz, T. Verlage

RWTH Aachen University, III. Physikalisches Institut A, Aachen, Germany

A. Albert, M. Brodski, E. Dietz-Laursonn, D. Duchardt, M. Endres, M. Erdmann, S. Erdweg, T. Esch, R. Fischer, A. Güth, M. Hamer, T. Hebbeker, C. Heidemann, K. Hoepfner, S. Knutzen, M. Merschmeyer, A. Meyer, P. Millet, S. Mukherjee, M. Olschewski, K. Padeken, T. Pook, M. Radziej, H. Reithler, M. Rieger, F. Scheuch, D. Teyssier, S. Thüer

RWTH Aachen University, III. Physikalisches Institut B, Aachen, GermanyG. Flügge, B. Kargoll, T. Kress, A. Künsken, J. Lingemann, T. Müller, A. Nehrkorn, A. Nowack, C. Pistone, O. Pooth, A. Stahl¹⁵**Deutsches Elektronen-Synchrotron, Hamburg, Germany**M. Aldaya Martin, T. Arndt, C. Asawatangtrakuldee, K. Beernaert, O. Behnke, U. Behrens, A. Bermúdez Martínez, A.A. Bin Anuar, K. Borras¹⁶, V. Botta, A. Campbell, P. Connor, C. Contreras-Campana, F. Costanza, C. Diez Pardos, G. Eckerlin, D. Eckstein, T. Eichhorn,

E. Eren, E. Gallo¹⁷, J. Garay Garcia, A. Geiser, A. Gzhko, J.M. Grados Luyando, A. Grohsjean, P. Gunnellini, A. Harb, J. Hauk, M. Hempel¹⁸, H. Jung, A. Kalogeropoulos, M. Kasemann, J. Keaveney, C. Kleinwort, I. Korol, D. Krücker, W. Lange, A. Lelek, T. Lenz, J. Leonard, K. Lipka, W. Lohmann¹⁸, R. Mankel, I.-A. Melzer-Pellmann, A.B. Meyer, G. Mittag, J. Mnich, A. Mussgiller, E. Ntomari, D. Pitzl, R. Placakyte, A. Raspereza, B. Roland, M. Savitskyi, P. Saxena, R. Shevchenko, S. Spannagel, N. Stefaniuk, G.P. Van Onsem, R. Walsh, Y. Wen, K. Wichmann, C. Wissing, O. Zenaiev

University of Hamburg, Hamburg, Germany

S. Bein, V. Blobel, M. Centis Vignali, A.R. Draeger, T. Dreyer, E. Garutti, D. Gonzalez, J. Haller, A. Hinzmann, M. Hoffmann, A. Karavdina, R. Klanner, R. Kogler, N. Kovalchuk, S. Kurz, T. Lapsien, I. Marchesini, D. Marconi, M. Meyer, M. Niedziela, D. Nowatschin, F. Pantaleo¹⁵, T. Peiffer, A. Perieanu, C. Scharf, P. Schleper, A. Schmidt, S. Schumann, J. Schwandt, J. Sonneveld, H. Stadie, G. Steinbrück, F.M. Stober, M. Stöver, H. Tholen, D. Troendle, E. Usai, L. Vanelderen, A. Vanhoefer, B. Vormwald

Institut für Experimentelle Kernphysik, Karlsruhe, Germany

M. Akbiyik, C. Barth, S. Baur, E. Butz, R. Caspart, T. Chwalek, F. Colombo, W. De Boer, A. Dierlamm, B. Freund, R. Friese, M. Giffels, A. Gilbert, D. Haitz, F. Hartmann¹⁵, S.M. Heindl, U. Husemann, F. Kassel¹⁵, S. Kudella, H. Mildner, M.U. Mozer, Th. Müller, M. Plagge, G. Quast, K. Rabbertz, M. Schröder, I. Shvetsov, G. Sieber, H.J. Simonis, R. Ulrich, S. Wayand, M. Weber, T. Weiler, S. Williamson, C. Wöhrmann, R. Wolf

Institute of Nuclear and Particle Physics (INPP), NCSR Demokritos, Aghia Paraskevi, Greece

G. Anagnostou, G. Daskalakis, T. Geralis, V.A. Giakoumopoulou, A. Kyriakis, D. Loukas, I. Topsis-Giotis

National and Kapodistrian University of Athens, Athens, Greece

S. Kesisoglou, A. Panagiotou, N. Saoulidou

University of Ioánnina, Ioánnina, Greece

I. Evangelou, C. Foudas, P. Kokkas, N. Manthos, I. Papadopoulos, E. Paradas, J. Strologas, F.A. Triantis

MTA-ELTE Lendület CMS Particle and Nuclear Physics Group, Eötvös Loránd University, Budapest, Hungary

M. Csanad, N. Filipovic, G. Pasztor

Wigner Research Centre for Physics, Budapest, Hungary

G. Bencze, C. Hajdu, D. Horvath¹⁹, Á. Hunyadi, F. Sikler, V. Veszpremi, G. Vesztregombi²⁰, A.J. Zsigmond

Institute of Nuclear Research ATOMKI, Debrecen, Hungary

N. Beni, S. Czellar, J. Karancsi²¹, A. Makovec, J. Molnar, Z. Szillasi

Institute of Physics, University of Debrecen, Debrecen, Hungary

M. Bartók²⁰, P. Raics, Z.L. Trocsanyi, B. Ujvari

Indian Institute of Science (IISc), Bangalore, India

S. Choudhury, J.R. Komaragiri

National Institute of Science Education and Research, Bhubaneswar, India

S. Bahinipati²², S. Bhowmik, P. Mal, K. Mandal, A. Nayak²³, D.K. Sahoo²², N. Sahoo, S.K. Swain

Panjab University, Chandigarh, India

S. Bansal, S.B. Beri, V. Bhatnagar, U. Bhawandeep, R. Chawla, N. Dhingra, A.K. Kalsi, A. Kaur, M. Kaur, R. Kumar, P. Kumari, A. Mehta, J.B. Singh, G. Walia

University of Delhi, Delhi, India

Ashok Kumar, Aashaq Shah, A. Bhardwaj, S. Chauhan, B.C. Choudhary, R.B. Garg, S. Keshri, A. Kumar, S. Malhotra, M. Naimuddin, K. Ranjan, R. Sharma, V. Sharma

Saha Institute of Nuclear Physics, HBNI, Kolkata, India

R. Bhardwaj, R. Bhattacharya, S. Bhattacharya, S. Dey, S. Dutt, S. Dutta, S. Ghosh, N. Majumdar, A. Modak, K. Mondal, S. Mukhopadhyay, S. Nandan, A. Purohit, A. Roy, D. Roy, S. Roy Chowdhury, S. Sarkar, M. Sharan, S. Thakur

Indian Institute of Technology Madras, Madras, India

P.K. Behera

Bhabha Atomic Research Centre, Mumbai, India

R. Chudasama, D. Dutta, V. Jha, V. Kumar, A.K. Mohanty¹⁵, P.K. Netrakanti, L.M. Pant, P. Shukla, A. Topkar

Tata Institute of Fundamental Research-A, Mumbai, India

T. Aziz, S. Dugad, B. Mahakud, S. Mitra, G.B. Mohanty, B. Parida, N. Sur, B. Sutar

Tata Institute of Fundamental Research-B, Mumbai, India

S. Banerjee, S. Bhattacharya, S. Chatterjee, P. Das, M. Guchait, Sa. Jain, S. Kumar, M. Maity²⁴, G. Majumder, K. Mazumdar, T. Sarkar²⁴, N. Wickramage²⁵

Indian Institute of Science Education and Research (IISER), Pune, India

S. Chauhan, S. Dube, V. Hegde, A. Kapoor, K. Kothekar, S. Pandey, A. Rane, S. Sharma

Institute for Research in Fundamental Sciences (IPM), Tehran, Iran

S. Chenarani²⁶, E. Eskandari Tadavani, S.M. Etesami²⁶, M. Khakzad, M. Mohammadi Najafabadi, M. Naseri, S. Pakhtinat Mehdiabadi²⁷, F. Rezaei Hosseinabadi, B. Safarzadeh²⁸, M. Zeinali

University College Dublin, Dublin, Ireland

M. Felcini, M. Grunewald

INFN Sezione di Bari ^a, Università di Bari ^b, Politecnico di Bari ^c, Bari, Italy

M. Abbrescia^{a,b}, C. Calabria^{a,b}, C. Caputo^{a,b}, A. Colaleo^a, D. Creanza^{a,c}, L. Cristella^{a,b}, N. De Filippis^{a,c}, M. De Palma^{a,b}, F. Errico^{a,b}, L. Fiore^a, G. Iaselli^{a,c}, S. Lezki^{a,b}, G. Maggi^{a,c}, M. Maggi^a, G. Miniello^{a,b}, S. My^{a,b}, S. Nuzzo^{a,b}, A. Pompili^{a,b}, G. Pugliese^{a,c}, R. Radogna^{a,b}, A. Ranieri^a, G. Selvaggi^{a,b}, A. Sharma^a, L. Silvestris^{a,15}, R. Venditti^a, P. Verwilligen^a

INFN Sezione di Bologna ^a, Università di Bologna ^b, Bologna, Italy

G. Abbiendi^a, C. Battilana^{a,b}, D. Bonacorsi^{a,b}, S. Braibant-Giacomelli^{a,b}, R. Campanini^{a,b}, P. Capiluppi^{a,b}, A. Castro^{a,b}, F.R. Cavallo^a, S.S. Chhibra^a, G. Codispoti^{a,b}, M. Cuffiani^{a,b}, G.M. Dallavalle^a, F. Fabbri^a, A. Fanfani^{a,b}, D. Fasanella^{a,b}, P. Giacomelli^a, C. Grandi^a, L. Guiducci^{a,b}, S. Marcellini^a, G. Masetti^a, A. Montanari^a, F.L. Navarria^{a,b}, A. Perrotta^a, A.M. Rossi^{a,b}, T. Rovelli^{a,b}, G.P. Siroli^{a,b}, N. Tosi^a

INFN Sezione di Catania ^a, Università di Catania ^b, Catania, Italy

S. Albergo^{a,b}, S. Costa^{a,b}, A. Di Mattia^a, F. Giordano^{a,b}, R. Potenza^{a,b}, A. Tricomi^{a,b}, C. Tuve^{a,b}

INFN Sezione di Firenze ^a, Università di Firenze ^b, Firenze, Italy

G. Barbagli^a, K. Chatterjee^{a,b}, V. Ciulli^{a,b}, C. Civinini^a, R. D'Alessandro^{a,b}, E. Focardi^{a,b}, P. Lenzi^{a,b}, M. Meschini^a, L. Russo^{a,29}, G. Sguazzoni^a, D. Strom^a, L. Viliani^{a,b,15}

INFN Laboratori Nazionali di Frascati, Frascati, Italy

L. Benussi, S. Bianco, F. Fabbri, D. Piccolo, F. Primavera¹⁵

INFN Sezione di Genova ^a, Università di Genova ^b, Genova, Italy

V. Calvelli^{a,b}, F. Ferro^a, E. Robutti^a, S. Tosi^{a,b}

INFN Sezione di Milano-Bicocca ^a, Università di Milano-Bicocca ^b, Milano, Italy

L. Brianza^{a,b}, F. Brivio^{a,b}, V. Ciriolo^{a,b}, M.E. Dinardo^{a,b}, S. Fiorendi^{a,b}, S. Gennai^a, A. Ghezzi^{a,b}, P. Govoni^{a,b}, M. Malberti^{a,b}, S. Malvezzi^a, R.A. Manzoni^{a,b}, D. Menasce^a, L. Moroni^a, M. Paganoni^{a,b}, K. Pauwels^{a,b}, D. Pedrini^a, S. Pigazzini^{a,b,30}, S. Ragazzi^{a,b}, T. Tabarelli de Fatis^{a,b}

INFN Sezione di Napoli ^a, Università di Napoli 'Federico II' ^b, Napoli, Italy, Università della Basilicata ^c, Potenza, Italy, Università G. Marconi ^d, Roma, Italy

S. Buontempo^a, N. Cavallo^{a,c}, S. Di Guida^{a,d,15}, M. Esposito^{a,b}, F. Fabozzi^{a,c}, F. Fienga^{a,b}, A.O.M. Iorio^{a,b}, W.A. Khan^a, G. Lanza^a, L. Lista^a, S. Meola^{a,d,15}, P. Paolucci^{a,15}, C. Sciacca^{a,b}, F. Thyssen^a

INFN Sezione di Padova ^a, Università di Padova ^b, Padova, Italy, Università di Trento ^c, Trento, Italy

P. Azzi^{a,15}, N. Bacchetta^a, L. Benato^{a,b}, D. Bisello^{a,b}, A. Boletti^{a,b}, R. Carlin^{a,b}, A. Carvalho Antunes De Oliveira^{a,b}, P. Checchia^a, P. De Castro Manzano^a, T. Dorigo^a, U. Dosselli^a, F. Gasparini^{a,b}, U. Gasparini^{a,b}, A. Gozzelino^a, S. Lacaprara^a, M. Margoni^{a,b}, A.T. Meneguzzo^{a,b}, N. Pozzobon^{a,b}, P. Ronchese^{a,b}, R. Rossin^{a,b}, F. Simonetto^{a,b}, E. Torassa^a, M. Zanetti^{a,b}, P. Zotto^{a,b}, G. Zumerle^{a,b}

INFN Sezione di Pavia ^a, Università di Pavia ^b, Pavia, Italy

A. Braghieri^a, F. Fallavollita^{a,b}, A. Magnani^{a,b}, P. Montagna^{a,b}, S.P. Ratti^{a,b}, V. Re^a, M. Ressegotti, C. Riccardi^{a,b}, P. Salvini^a, I. Vai^{a,b}, P. Vitulo^{a,b}

INFN Sezione di Perugia ^a, Università di Perugia ^b, Perugia, Italy

L. Alunni Solestizi^{a,b}, M. Biasini^{a,b}, G.M. Bilei^a, C. Cecchi^{a,b}, D. Ciangottini^{a,b}, L. Fanò^{a,b}, P. Lariccia^{a,b}, R. Leonardi^{a,b}, E. Manoni^a, G. Mantovani^{a,b}, V. Mariani^{a,b}, M. Menichelli^a, A. Rossi^{a,b}, A. Santocchia^{a,b}, D. Spiga^a

INFN Sezione di Pisa ^a, Università di Pisa ^b, Scuola Normale Superiore di Pisa ^c, Pisa, Italy

K. Androsov^a, P. Azzurri^{a,15}, G. Bagliesi^a, J. Bernardini^a, T. Boccali^a, L. Borrello, R. Castaldi^a, M.A. Ciocci^{a,b}, R. Dell'Orso^a, G. Fedi^a, L. Giannini^{a,c}, A. Giassi^a, M.T. Grippo^{a,29}, F. Ligabue^{a,c}, T. Lomtadze^a, E. Manca^{a,c}, G. Mandorli^{a,c}, L. Martini^{a,b}, A. Messineo^{a,b}, F. Palla^a, A. Rizzi^{a,b}, A. Savoy-Navarro^{a,31}, P. Spagnolo^a, R. Tenchini^a, G. Tonelli^{a,b}, A. Venturi^a, P.G. Verdini^a

INFN Sezione di Roma ^a, Sapienza Università di Roma ^b, Rome, Italy

L. Barone^{a,b}, F. Cavallari^a, M. Cipriani^{a,b}, D. Del Re^{a,b,15}, M. Diemoz^a, S. Gelli^{a,b}, E. Longo^{a,b}, F. Margaroli^{a,b}, B. Marzocchi^{a,b}, P. Meridiani^a, G. Organtini^{a,b}, R. Paramatti^{a,b}, F. Preiato^{a,b}, S. Rahatlou^{a,b}, C. Rovelli^a, F. Santanastasio^{a,b}

INFN Sezione di Torino ^a, Università di Torino ^b, Torino, Italy, Università del Piemonte Orientale ^c, Novara, Italy

N. Amapane^{a,b}, R. Arcidiacono^{a,c}, S. Argiro^{a,b}, M. Arneodo^{a,c}, N. Bartosik^a, R. Bellan^{a,b}, C. Biino^a, N. Cartiglia^a, F. Cenna^{a,b}, M. Costa^{a,b}, R. Covarelli^{a,b}, A. Degano^{a,b}, N. Demaria^a,

B. Kiani^{a,b}, C. Mariotti^a, S. Maselli^a, E. Migliore^{a,b}, V. Monaco^{a,b}, E. Monteil^{a,b}, M. Monteno^a, M.M. Obertino^{a,b}, L. Pacher^{a,b}, N. Pastrone^a, M. Pelliccioni^a, G.L. Pinna Angioni^{a,b}, F. Ravera^{a,b}, A. Romero^{a,b}, M. Ruspa^{a,c}, R. Sacchi^{a,b}, K. Shchelina^{a,b}, V. Sola^a, A. Solano^{a,b}, A. Staiano^a, P. Traczyk^{a,b}

INFN Sezione di Trieste ^a, Università di Trieste ^b, Trieste, Italy
S. Belforte^a, M. Casarsa^a, F. Cossutti^a, G. Della Ricca^{a,b}, A. Zanetti^a

Kyungpook National University, Daegu, Korea

D.H. Kim, G.N. Kim, M.S. Kim, J. Lee, S. Lee, S.W. Lee, C.S. Moon, Y.D. Oh, S. Sekmen, D.C. Son, Y.C. Yang

Chonbuk National University, Jeonju, Korea

A. Lee

Chonnam National University, Institute for Universe and Elementary Particles, Kwangju, Korea

H. Kim, D.H. Moon, G. Oh

Hanyang University, Seoul, Korea

J.A. Brochero Cifuentes, J. Goh, T.J. Kim

Korea University, Seoul, Korea

S. Cho, S. Choi, Y. Go, D. Gyun, S. Ha, B. Hong, Y. Jo, Y. Kim, K. Lee, K.S. Lee, S. Lee, J. Lim, S.K. Park, Y. Roh

Seoul National University, Seoul, Korea

J. Almond, J. Kim, J.S. Kim, H. Lee, K. Lee, K. Nam, S.B. Oh, B.C. Radburn-Smith, S.h. Seo, U.K. Yang, H.D. Yoo, G.B. Yu

University of Seoul, Seoul, Korea

M. Choi, H. Kim, J.H. Kim, J.S.H. Lee, I.C. Park, G. Ryu

Sungkyunkwan University, Suwon, Korea

Y. Choi, C. Hwang, J. Lee, I. Yu

Vilnius University, Vilnius, Lithuania

V. Dudenas, A. Juodagalvis, J. Vaitkus

National Centre for Particle Physics, Universiti Malaya, Kuala Lumpur, Malaysia

I. Ahmed, Z.A. Ibrahim, M.A.B. Md Ali³², F. Mohamad Idris³³, W.A.T. Wan Abdullah, M.N. Yusli, Z. Zolkapli

Centro de Investigacion y de Estudios Avanzados del IPN, Mexico City, Mexico

H. Castilla-Valdez, E. De La Cruz-Burelo, I. Heredia-De La Cruz³⁴, R. Lopez-Fernandez, J. Mejia Guisao, A. Sanchez-Hernandez

Universidad Iberoamericana, Mexico City, Mexico

S. Carrillo Moreno, C. Oropeza Barrera, F. Vazquez Valencia

Benemerita Universidad Autonoma de Puebla, Puebla, Mexico

I. Pedraza, H.A. Salazar Ibarguen, C. Uribe Estrada

Universidad Autónoma de San Luis Potosí, San Luis Potosí, Mexico

A. Morelos Pineda

University of Auckland, Auckland, New Zealand

D. Kofcheck

University of Canterbury, Christchurch, New Zealand

P.H. Butler

National Centre for Physics, Quaid-I-Azam University, Islamabad, Pakistan

A. Ahmad, M. Ahmad, Q. Hassan, H.R. Hoorani, A. Saddique, M.A. Shah, M. Shoaib, M. Waqas

National Centre for Nuclear Research, Swierk, Poland

H. Bialkowska, M. Bluj, B. Boimska, T. Frueboes, M. Górski, M. Kazana, K. Nawrocki, K. Romanowska-Rybinska, M. Szleper, P. Zalewski

Institute of Experimental Physics, Faculty of Physics, University of Warsaw, Warsaw, PolandK. Bunkowski, A. Byszuk³⁵, K. Doroba, A. Kalinowski, M. Konecki, J. Krolikowski, M. Misiura, M. Olszewski, A. Pyskir, M. Walczak**Laboratório de Instrumentação e Física Experimental de Partículas, Lisboa, Portugal**

P. Bargassa, C. Beirão Da Cruz E Silva, B. Calpas, A. Di Francesco, P. Faccioli, M. Gallinaro, J. Hollar, N. Leonardo, L. Lloret Iglesias, M.V. Nemallapudi, J. Seixas, O. Toldaiev, D. Vadruccio, J. Varela

Joint Institute for Nuclear Research, Dubna, RussiaS. Afanasiev, P. Bunin, M. Gavrilenco, I. Golutvin, I. Gorbunov, A. Kamenev, V. Karjavin, A. Lanev, A. Malakhov, V. Matveev^{36,37}, V. Palichik, V. Perelygin, S. Shmatov, S. Shulha, N. Skatchkov, V. Smirnov, N. Voityshin, A. Zarubin**Petersburg Nuclear Physics Institute, Gatchina (St. Petersburg), Russia**Y. Ivanov, V. Kim³⁸, E. Kuznetsova³⁹, P. Levchenko, V. Murzin, V. Oreshkin, I. Smirnov, V. Sulimov, L. Uvarov, S. Vavilov, A. Vorobyev**Institute for Nuclear Research, Moscow, Russia**

Yu. Andreev, A. Dermenev, S. Gninenko, N. Golubev, A. Karneyeu, M. Kirsanov, N. Krasnikov, A. Pashenkov, D. Tlisov, A. Toropin

Institute for Theoretical and Experimental Physics, Moscow, Russia

V. Epshteyn, V. Gavrilov, N. Lychkovskaya, V. Popov, I. Pozdnyakov, G. Safronov, A. Spiridonov, A. Stepennov, M. Toms, E. Vlasov, A. Zhokin

Moscow Institute of Physics and Technology, Moscow, RussiaT. Aushev, A. Bylinkin³⁷**National Research Nuclear University 'Moscow Engineering Physics Institute' (MEPhI), Moscow, Russia**R. Chistov⁴⁰, M. Danilov⁴⁰, P. Parygin, D. Philippov, S. Polikarpov, E. Tarkovskii**P.N. Lebedev Physical Institute, Moscow, Russia**V. Andreev, M. Azarkin³⁷, I. Dremin³⁷, M. Kirakosyan³⁷, A. Terkulov**Skobeltsyn Institute of Nuclear Physics, Lomonosov Moscow State University, Moscow, Russia**A. Baskakov, A. Belyaev, E. Boos, M. Dubinin⁴¹, L. Dudko, A. Ershov, A. Gribushin, V. Klyukhin, O. Kodolova, I. Lokhtin, I. Miagkov, S. Obraztsov, S. Petrushanko, V. Savrin, A. Snigirev

Novosibirsk State University (NSU), Novosibirsk, RussiaV. Blinov⁴², Y. Skovpen⁴², D. Shtol⁴²**State Research Center of Russian Federation, Institute for High Energy Physics, Protvino, Russia**

I. Azhgirey, I. Bayshev, S. Bitiukov, D. Elumakhov, V. Kachanov, A. Kalinin, D. Konstantinov, V. Krychkine, V. Petrov, R. Ryutin, A. Sobol, S. Troshin, N. Tyurin, A. Uzunian, A. Volkov

University of Belgrade, Faculty of Physics and Vinca Institute of Nuclear Sciences, Belgrade, SerbiaP. Adzic⁴³, P. Cirkovic, D. Devetak, M. Dordevic, J. Milosevic, V. Rekovic**Centro de Investigaciones Energéticas Medioambientales y Tecnológicas (CIEMAT), Madrid, Spain**

J. Alcaraz Maestre, M. Barrio Luna, M. Cerrada, N. Colino, B. De La Cruz, A. Delgado Peris, A. Escalante Del Valle, C. Fernandez Bedoya, J.P. Fernández Ramos, J. Flix, M.C. Fouz, P. Garcia-Abia, O. Gonzalez Lopez, S. Goy Lopez, J.M. Hernandez, M.I. Josa, A. Pérez-Calero Yzquierdo, J. Puerta Pelayo, A. Quintario Olmeda, I. Redondo, L. Romero, M.S. Soares, A. Álvarez Fernández

Universidad Autónoma de Madrid, Madrid, Spain

J.F. de Trocóniz, M. Missiroli, D. Moran

Universidad de Oviedo, Oviedo, Spain

J. Cuevas, C. Erice, J. Fernandez Menendez, I. Gonzalez Caballero, J.R. González Fernández, E. Palencia Cortezon, S. Sanchez Cruz, I. Suárez Andrés, P. Vischia, J.M. Vizan Garcia

Instituto de Física de Cantabria (IFCA), CSIC-Universidad de Cantabria, Santander, Spain

I.J. Cabrillo, A. Calderon, B. Chazin Quero, E. Curras, M. Fernandez, J. Garcia-Ferrero, G. Gomez, A. Lopez Virtu, J. Marco, C. Martinez Rivero, P. Martinez Ruiz del Arbol, F. Matorras, J. Piedra Gomez, T. Rodrigo, A. Ruiz-Jimeno, L. Scodellaro, N. Trevisani, I. Vila, R. Vilar Cortabitarte

CERN, European Organization for Nuclear Research, Geneva, SwitzerlandD. Abbaneo, E. Auffray, P. Baillon, A.H. Ball, D. Barney, M. Bianco, P. Bloch, A. Bocci, C. Botta, T. Camporesi, R. Castello, M. Cepeda, G. Cerminara, E. Chapon, Y. Chen, D. d'Enterria, A. Dabrowski, V. Daponte, A. David, M. De Gruttola, A. De Roeck, E. Di Marco⁴⁴, M. Dobson, B. Dorney, T. du Pree, M. Dünser, N. Dupont, A. Elliott-Peisert, P. Everaerts, G. Franzoni, J. Fulcher, W. Funk, D. Gigi, K. Gill, F. Glege, D. Gulhan, S. Gundacker, M. Guthoff, P. Harris, J. Hegeman, V. Innocente, P. Janot, O. Karacheban¹⁸, J. Kieseler, H. Kirschenmann, V. Knünz, A. Kornmayer¹⁵, M.J. Kortelainen, C. Lange, P. Lecoq, C. Lourenço, M.T. Lucchini, L. Malgeri, M. Mannelli, A. Martelli, F. Meijers, J.A. Merlin, S. Mersi, E. Meschi, P. Milenovic⁴⁵, F. Moortgat, M. Mulders, H. Neugebauer, S. Orfanelli, L. Orsini, L. Pape, E. Perez, M. Peruzzi, A. Petrilli, G. Petrucciani, A. Pfeiffer, M. Pierini, A. Racz, T. Reis, G. Roland⁴⁶, M. Rovere, H. Sakulin, C. Schäfer, C. Schwick, M. Seidel, M. Selvaggi, A. Sharma, P. Silva, P. Sphicas⁴⁷, J. Steggemann, M. Stoye, M. Tosi, D. Treille, A. Triossi, A. Tsirou, V. Veckalns⁴⁸, G.I. Veres²⁰, M. Verweij, N. Wardle, W.D. Zeuner**Paul Scherrer Institut, Villigen, Switzerland**W. Bertl[†], L. Caminada⁴⁹, K. Deiters, W. Erdmann, R. Horisberger, Q. Ingram, H.C. Kaestli, D. Kotlinski, U. Langenegger, T. Rohe, S.A. Wiederkehr**Institute for Particle Physics, ETH Zurich, Zurich, Switzerland**

F. Bachmair, L. Bäni, P. Berger, L. Bianchini, B. Casal, G. Dissertori, M. Dittmar, M. Donegà,

C. Grab, C. Heidegger, D. Hits, J. Hoss, G. Kasiczka, T. Klijnsma, W. Lustermann, B. Mangano, M. Marionneau, M.T. Meinhard, D. Meister, F. Micheli, P. Musella, F. Nessi-Tedaldi, F. Pandolfi, J. Pata, F. Pauss, G. Perrin, L. Perrozzi, M. Quitnat, M. Schönenberger, L. Shchutska, V.R. Tavolaro, K. Theofilatos, M.L. Vesterbacka Olsson, R. Wallny, A. Zagozdzinska³⁵, D.H. Zhu

Universität Zürich, Zurich, Switzerland

T.K. Arrestad, C. Amsler⁵⁰, M.F. Canelli, A. De Cosa, S. Donato, C. Galloni, T. Hreus, B. Kilminster, J. Ngadiuba, D. Pinna, G. Rauco, P. Robmann, D. Salerno, C. Seitz, A. Zucchetta

National Central University, Chung-Li, Taiwan

V. Candelise, T.H. Doan, Sh. Jain, R. Khurana, C.M. Kuo, W. Lin, A. Pozdnyakov, S.S. Yu

National Taiwan University (NTU), Taipei, Taiwan

Arun Kumar, P. Chang, Y. Chao, K.F. Chen, P.H. Chen, F. Fiori, W.-S. Hou, Y. Hsiung, Y.F. Liu, R.-S. Lu, M. Miñano Moya, E. Paganis, A. Psallidas, J.f. Tsai

Chulalongkorn University, Faculty of Science, Department of Physics, Bangkok, Thailand

B. Asavapibhop, K. Kovitanggoon, G. Singh, N. Srimanobhas

ukurova University, Physics Department, Science and Art Faculty, Adana, Turkey

A. Adiguzel⁵¹, M.N. Bakirci⁵², F. Boran, S. Damarseckin, Z.S. Demiroglu, C. Dozen, E. Eskut, S. Girgis, G. Gokbulut, Y. Guler, I. Hos⁵³, E.E. Kangal⁵⁴, O. Kara, U. Kiminsu, M. Oglakci, G. Onengut⁵⁵, K. Ozdemir⁵⁶, S. Ozturk⁵², A. Polatoz, D. Sunar Cerci⁵⁷, S. Turkcapar, I.S. Zorbakir, C. Zorbilmez

Middle East Technical University, Physics Department, Ankara, Turkey

B. Bilin, G. Karapinar⁵⁸, K. Ocalan⁵⁹, M. Yalvac, M. Zeyrek

Bogazici University, Istanbul, Turkey

E. Gürmez, M. Kaya⁶⁰, O. Kaya⁶¹, S. Tekten, E.A. Yetkin⁶²

Istanbul Technical University, Istanbul, Turkey

M.N. Agaras, S. Atay, A. Cakir, K. Cankocak

Institute for Scintillation Materials of National Academy of Science of Ukraine, Kharkov, Ukraine

B. Grynyov

National Scientific Center, Kharkov Institute of Physics and Technology, Kharkov, Ukraine

L. Levchuk, P. Sorokin

University of Bristol, Bristol, United Kingdom

R. Aggleton, F. Ball, L. Beck, J.J. Brooke, D. Burns, E. Clement, D. Cussans, O. Davignon, H. Flacher, J. Goldstein, M. Grimes, G.P. Heath, H.F. Heath, J. Jacob, L. Kreczko, C. Lucas, D.M. Newbold⁶³, S. Paramesvaran, A. Poll, T. Sakuma, S. Seif El Nasr-storey, D. Smith, V.J. Smith

Rutherford Appleton Laboratory, Didcot, United Kingdom

K.W. Bell, A. Belyaev⁶⁴, C. Brew, R.M. Brown, L. Calligaris, D. Cieri, D.J.A. Cockerill, J.A. Coughlan, K. Harder, S. Harper, E. Olaiya, D. Petyt, C.H. Shepherd-Themistocleous, A. Thea, I.R. Tomalin, T. Williams

Imperial College, London, United Kingdom

R. Bainbridge, S. Breeze, O. Buchmuller, A. Bundock, S. Casasso, M. Citron, D. Colling, L. Corpe, P. Dauncey, G. Davies, A. De Wit, M. Della Negra, R. Di Maria, A. Elwood, Y. Haddad, G. Hall, G. Iles, T. James, R. Lane, C. Laner, L. Lyons, A.-M. Magnan, S. Malik, L. Mastrolorenzo,

T. Matsushita, J. Nash, A. Nikitenko⁶, V. Palladino, M. Pesaresi, D.M. Raymond, A. Richards, A. Rose, E. Scott, C. Seez, A. Shtipliyski, S. Summers, A. Tapper, K. Uchida, M. Vazquez Acosta⁶⁵, T. Virdee¹⁵, D. Winterbottom, J. Wright, S.C. Zenz

Brunel University, Uxbridge, United Kingdom

J.E. Cole, P.R. Hobson, A. Khan, P. Kyberd, I.D. Reid, P. Symonds, L. Teodorescu, M. Turner

Baylor University, Waco, USA

A. Borzou, K. Call, J. Dittmann, K. Hatakeyama, H. Liu, N. Pastika, C. Smith

Catholic University of America, Washington DC, USA

R. Bartek, A. Dominguez

The University of Alabama, Tuscaloosa, USA

A. Buccilli, S.I. Cooper, C. Henderson, P. Rumerio, C. West

Boston University, Boston, USA

D. Arcaro, A. Avetisyan, T. Bose, D. Gastler, D. Rankin, C. Richardson, J. Rohlf, L. Sulak, D. Zou

Brown University, Providence, USA

G. Benelli, D. Cutts, A. Garabedian, J. Hakala, U. Heintz, J.M. Hogan, K.H.M. Kwok, E. Laird, G. Landsberg, Z. Mao, M. Narain, J. Pazzini, S. Piperov, S. Sagir, R. Syarif, D. Yu

University of California, Davis, Davis, USA

R. Band, C. Brainerd, D. Burns, M. Calderon De La Barca Sanchez, M. Chertok, J. Conway, R. Conway, P.T. Cox, R. Erbacher, C. Flores, G. Funk, M. Gardner, W. Ko, R. Lander, C. Mclean, M. Mulhearn, D. Pellett, J. Pilot, S. Shalhout, M. Shi, J. Smith, M. Squires, D. Stolp, K. Tos, M. Tripathi, Z. Wang

University of California, Los Angeles, USA

M. Bachtis, C. Bravo, R. Cousins, A. Dasgupta, A. Florent, J. Hauser, M. Ignatenko, N. Mccoll, D. Saltzberg, C. Schnaible, V. Valuev

University of California, Riverside, Riverside, USA

E. Bouvier, K. Burt, R. Clare, J. Ellison, J.W. Gary, S.M.A. Ghiasi Shirazi, G. Hanson, J. Heilman, P. Jandir, E. Kennedy, F. Lacroix, O.R. Long, M. Olmedo Negrete, M.I. Paneva, A. Shrinivas, W. Si, L. Wang, H. Wei, S. Wimpenny, B. R. Yates

University of California, San Diego, La Jolla, USA

J.G. Branson, S. Cittolin, M. Derdzinski, B. Hashemi, A. Holzner, D. Klein, G. Kole, V. Krutelyov, J. Letts, I. Macneill, M. Masciovecchio, D. Olivito, S. Padhi, M. Pieri, M. Sani, V. Sharma, S. Simon, M. Tadel, A. Vartak, S. Wasserbaech⁶⁶, J. Wood, F. Würthwein, A. Yagil, G. Zevi Della Porta

University of California, Santa Barbara - Department of Physics, Santa Barbara, USA

N. Amin, R. Bhandari, J. Bradmiller-Feld, C. Campagnari, A. Dishaw, V. Dutta, M. Franco Sevilla, C. George, F. Golf, L. Gouskos, J. Gran, R. Heller, J. Incandela, S.D. Mullin, A. Ovcharova, H. Qu, J. Richman, D. Stuart, I. Suarez, J. Yoo

California Institute of Technology, Pasadena, USA

D. Anderson, J. Bendavid, A. Bornheim, J.M. Lawhorn, H.B. Newman, T. Nguyen, C. Pena, M. Spiropulu, J.R. Vlimant, S. Xie, Z. Zhang, R.Y. Zhu

Carnegie Mellon University, Pittsburgh, USA

M.B. Andrews, T. Ferguson, T. Mudholkar, M. Paulini, J. Russ, M. Sun, H. Vogel, I. Vorobiev, M. Weinberg

University of Colorado Boulder, Boulder, USA

J.P. Cumalat, W.T. Ford, F. Jensen, A. Johnson, M. Krohn, S. Leontsinis, T. Mulholland, K. Stenson, S.R. Wagner

Cornell University, Ithaca, USA

J. Alexander, J. Chaves, J. Chu, S. Dittmer, K. Mcdermott, N. Mirman, J.R. Patterson, A. Rinkevicius, A. Ryd, L. Skinnari, L. Soffi, S.M. Tan, Z. Tao, J. Thom, J. Tucker, P. Wittich, M. Zientek

Fermi National Accelerator Laboratory, Batavia, USA

S. Abdullin, M. Albrow, G. Apollinari, A. Apresyan, A. Apyan, S. Banerjee, L.A.T. Bauerick, A. Beretvas, J. Berryhill, P.C. Bhat, G. Bolla, K. Burkett, J.N. Butler, A. Canepa, G.B. Cerati, H.W.K. Cheung, F. Chlebana, M. Cremonesi, J. Duarte, V.D. Elvira, J. Freeman, Z. Gecse, E. Gottschalk, L. Gray, D. Green, S. Grünendahl, O. Gutsche, R.M. Harris, S. Hasegawa, J. Hirschauer, Z. Hu, B. Jayatilaka, S. Jindariani, M. Johnson, U. Joshi, B. Klima, B. Kreis, S. Lammel, D. Lincoln, R. Lipton, M. Liu, T. Liu, R. Lopes De Sá, J. Lykken, K. Maeshima, N. Magini, J.M. Marraffino, S. Maruyama, D. Mason, P. McBride, P. Merkel, S. Mrenna, S. Nahn, V. O'Dell, K. Pedro, O. Prokofyev, G. Rakness, L. Ristori, B. Schneider, E. Sexton-Kennedy, A. Soha, W.J. Spalding, L. Spiegel, S. Stoynev, J. Strait, N. Strobbe, L. Taylor, S. Tkaczyk, N.V. Tran, L. Uplegger, E.W. Vaandering, C. Vernieri, M. Verzocchi, R. Vidal, M. Wang, H.A. Weber, A. Whitbeck

University of Florida, Gainesville, USA

D. Acosta, P. Avery, P. Bortignon, D. Bourilkov, A. Brinkerhoff, A. Carnes, M. Carver, D. Curry, S. Das, R.D. Field, I.K. Furic, J. Konigsberg, A. Korytov, K. Kotov, P. Ma, K. Matchev, H. Mei, G. Mitselmakher, D. Rank, D. Sperka, N. Terentyev, L. Thomas, J. Wang, S. Wang, J. Yelton

Florida International University, Miami, USA

Y.R. Joshi, S. Linn, P. Markowitz, G. Martinez, J.L. Rodriguez

Florida State University, Tallahassee, USA

A. Ackert, T. Adams, A. Askew, S. Hagopian, V. Hagopian, K.F. Johnson, T. Kolberg, T. Perry, H. Prosper, A. Saha, A. Santra, R. Yohay

Florida Institute of Technology, Melbourne, USA

M.M. Baarmand, V. Bhopatkar, S. Colafranceschi, M. Hohlmann, D. Noonan, T. Roy, F. Yumiceva

University of Illinois at Chicago (UIC), Chicago, USA

M.R. Adams, L. Apanasevich, D. Berry, R.R. Betts, R. Cavanaugh, X. Chen, O. Evdokimov, C.E. Gerber, D.A. Hangal, D.J. Hofman, K. Jung, J. Kamin, I.D. Sandoval Gonzalez, M.B. Tonjes, H. Trauger, N. Varelas, H. Wang, Z. Wu, J. Zhang

The University of Iowa, Iowa City, USA

B. Bilki⁶⁷, W. Clarida, K. Dilsiz⁶⁸, S. Durgut, R.P. Gandrajula, M. Haytmyradov, V. Khristenko, J.-P. Merlo, H. Mermerkaya⁶⁹, A. Mestvirishvili, A. Moeller, J. Nachtman, H. Ogul⁷⁰, Y. Onel, F. Ozok⁷¹, A. Penzo, C. Snyder, E. Tiras, J. Wetzel, K. Yi

Johns Hopkins University, Baltimore, USA

B. Blumenfeld, A. Cocoros, N. Eminizer, D. Fehling, L. Feng, A.V. Gritsan, P. Maksimovic, J. Roskes, U. Sarica, M. Swartz, M. Xiao, C. You

The University of Kansas, Lawrence, USA

A. Al-bataineh, P. Baringer, A. Bean, S. Boren, J. Bowen, J. Castle, S. Khalil, A. Kropivnitskaya,

D. Majumder, W. Mcbrayer, M. Murray, C. Royon, S. Sanders, E. Schmitz, R. Stringer, J.D. Tapia Takaki, Q. Wang

Kansas State University, Manhattan, USA

A. Ivanov, K. Kaadze, Y. Maravin, A. Mohammadi, L.K. Saini, N. Skhirtladze, S. Toda

Lawrence Livermore National Laboratory, Livermore, USA

F. Rebassoo, D. Wright

University of Maryland, College Park, USA

C. Anelli, A. Baden, O. Baron, A. Belloni, B. Calvert, S.C. Eno, C. Ferraioli, N.J. Hadley, S. Jabeen, G.Y. Jeng, R.G. Kellogg, J. Kunkle, A.C. Mignerey, F. Ricci-Tam, Y.H. Shin, A. Skuja, S.C. Tonwar

Massachusetts Institute of Technology, Cambridge, USA

D. Abercrombie, B. Allen, V. Azzolini, R. Barbieri, A. Baty, R. Bi, S. Brandt, W. Busza, I.A. Cali, M. D'Alfonso, Z. Demiragli, G. Gomez Ceballos, M. Goncharov, D. Hsu, Y. Iiyama, G.M. Innocenti, M. Klute, D. Kovalevskyi, Y.S. Lai, Y.-J. Lee, A. Levin, P.D. Luckey, B. Maier, A.C. Marini, C. McGinn, C. Mironov, S. Narayanan, X. Niu, C. Paus, C. Roland, G. Roland, J. Salfeld-Nebgen, G.S.F. Stephans, K. Tatar, D. Velicanu, J. Wang, T.W. Wang, B. Wyslouch

University of Minnesota, Minneapolis, USA

A.C. Benvenuti, R.M. Chatterjee, A. Evans, P. Hansen, S. Kalafut, Y. Kubota, Z. Lesko, J. Mans, S. Nourbakhsh, N. Ruckstuhl, R. Rusack, J. Turkewitz

University of Mississippi, Oxford, USA

J.G. Acosta, S. Oliveros

University of Nebraska-Lincoln, Lincoln, USA

E. Avdeeva, K. Bloom, D.R. Claes, C. Fangmeier, R. Gonzalez Suarez, R. Kamalieddin, I. Kravchenko, J. Monroy, J.E. Siado, G.R. Snow, B. Stieger

State University of New York at Buffalo, Buffalo, USA

M. Alyari, J. Dolen, A. Godshalk, C. Harrington, I. Iashvili, D. Nguyen, A. Parker, S. Rappoccio, B. Roozbahani

Northeastern University, Boston, USA

G. Alverson, E. Barberis, A. Hortiangtham, A. Massironi, D.M. Morse, D. Nash, T. Orimoto, R. Teixeira De Lima, D. Trocino, R.-J. Wang, D. Wood

Northwestern University, Evanston, USA

S. Bhattacharya, O. Charaf, K.A. Hahn, N. Mucia, N. Odell, B. Pollack, M.H. Schmitt, K. Sung, M. Trovato, M. Velasco

University of Notre Dame, Notre Dame, USA

N. Dev, M. Hildreth, K. Hurtado Anampa, C. Jessop, D.J. Karmgard, N. Kellams, K. Lannon, N. Loukas, N. Marinelli, F. Meng, C. Mueller, Y. Musienko³⁶, M. Planer, A. Reinsvold, R. Ruchti, G. Smith, S. Taroni, M. Wayne, M. Wolf, A. Woodard

The Ohio State University, Columbus, USA

J. Alimena, L. Antonelli, B. Bylsma, L.S. Durkin, S. Flowers, B. Francis, A. Hart, C. Hill, W. Ji, B. Liu, W. Luo, D. Puigh, B.L. Winer, H.W. Wulsin

Princeton University, Princeton, USA

A. Benaglia, S. Cooperstein, O. Driga, P. Elmer, J. Hardenbrook, P. Hebda, S. Higginbotham,

D. Lange, J. Luo, D. Marlow, K. Mei, I. Ojalvo, J. Olsen, C. Palmer, P. Piroué, D. Stickland, C. Tully

University of Puerto Rico, Mayaguez, USA

S. Malik, S. Norberg

Purdue University, West Lafayette, USA

A. Barker, V.E. Barnes, S. Folgueras, L. Gutay, M.K. Jha, M. Jones, A.W. Jung, A. Khatiwada, D.H. Miller, N. Neumeister, C.C. Peng, J.F. Schulte, J. Sun, F. Wang, W. Xie

Purdue University Northwest, Hammond, USA

T. Cheng, N. Parashar, J. Stupak

Rice University, Houston, USA

A. Adair, B. Akgun, Z. Chen, K.M. Ecklund, F.J.M. Geurts, M. Guilbaud, W. Li, B. Michlin, M. Northup, B.P. Padley, J. Roberts, J. Rorie, Z. Tu, J. Zabel

University of Rochester, Rochester, USA

A. Bodek, P. de Barbaro, R. Demina, Y.t. Duh, T. Ferbel, M. Galanti, A. Garcia-Bellido, J. Han, O. Hindrichs, A. Khukhunaishvili, K.H. Lo, P. Tan, M. Verzetti

The Rockefeller University, New York, USA

R. Ciesielski, K. Goulianios, C. Mesropian

Rutgers, The State University of New Jersey, Piscataway, USA

A. Agapitos, J.P. Chou, Y. Gershtein, T.A. Gómez Espinosa, E. Halkiadakis, M. Heindl, E. Hughes, S. Kaplan, R. Kunnawalkam Elayavalli, S. Kyriacou, A. Lath, R. Montalvo, K. Nash, M. Osherson, H. Saka, S. Salur, S. Schnetzer, D. Sheffield, S. Somalwar, R. Stone, S. Thomas, P. Thomassen, M. Walker

University of Tennessee, Knoxville, USA

A.G. Delannoy, M. Foerster, J. Heideman, G. Riley, K. Rose, S. Spanier, K. Thapa

Texas A&M University, College Station, USA

O. Bouhali⁷², A. Castaneda Hernandez⁷², A. Celik, M. Dalchenko, M. De Mattia, A. Delgado, S. Dildick, R. Eusebi, J. Gilmore, T. Huang, T. Kamon⁷³, R. Mueller, Y. Pakhotin, R. Patel, A. Perloff, L. Perniè, D. Rathjens, A. Safonov, A. Tatarinov, K.A. Ulmer

Texas Tech University, Lubbock, USA

N. Akchurin, J. Damgov, F. De Guio, P.R. Dudero, J. Faulkner, E. Gurpinar, S. Kunori, K. Lamichhane, S.W. Lee, T. Libeiro, T. Peltola, S. Undleeb, I. Volobouev, Z. Wang

Vanderbilt University, Nashville, USA

S. Greene, A. Gurrola, R. Janjam, W. Johns, C. Maguire, A. Melo, H. Ni, P. Sheldon, S. Tuo, J. Velkovska, Q. Xu

University of Virginia, Charlottesville, USA

M.W. Arenton, P. Barria, B. Cox, R. Hirosky, A. Ledovskoy, H. Li, C. Neu, T. Sinthuprasith, X. Sun, Y. Wang, E. Wolfe, F. Xia

Wayne State University, Detroit, USA

C. Clarke, R. Harr, P.E. Karchin, J. Sturdy, S. Zaleski

University of Wisconsin - Madison, Madison, WI, USA

J. Buchanan, C. Caillol, S. Dasu, L. Dodd, S. Duric, B. Gomber, M. Grothe, M. Herndon,

A. Hervé, U. Hussain, P. Klabbers, A. Lanaro, A. Levine, K. Long, R. Loveless, G.A. Pierro, G. Polese, T. Ruggles, A. Savin, N. Smith, W.H. Smith, D. Taylor, N. Woods

†: Deceased

- 1: Also at Vienna University of Technology, Vienna, Austria
- 2: Also at State Key Laboratory of Nuclear Physics and Technology, Peking University, Beijing, China
- 3: Also at Universidade Estadual de Campinas, Campinas, Brazil
- 4: Also at Universidade Federal de Pelotas, Pelotas, Brazil
- 5: Also at Université Libre de Bruxelles, Bruxelles, Belgium
- 6: Also at Institute for Theoretical and Experimental Physics, Moscow, Russia
- 7: Also at Joint Institute for Nuclear Research, Dubna, Russia
- 8: Also at Suez University, Suez, Egypt
- 9: Now at British University in Egypt, Cairo, Egypt
- 10: Also at Fayoum University, El-Fayoum, Egypt
- 11: Now at Helwan University, Cairo, Egypt
- 12: Also at Université de Haute Alsace, Mulhouse, France
- 13: Also at Skobeltsyn Institute of Nuclear Physics, Lomonosov Moscow State University, Moscow, Russia
- 14: Also at Ilia State University, Tbilisi, Georgia
- 15: Also at CERN, European Organization for Nuclear Research, Geneva, Switzerland
- 16: Also at RWTH Aachen University, III. Physikalisches Institut A, Aachen, Germany
- 17: Also at University of Hamburg, Hamburg, Germany
- 18: Also at Brandenburg University of Technology, Cottbus, Germany
- 19: Also at Institute of Nuclear Research ATOMKI, Debrecen, Hungary
- 20: Also at MTA-ELTE Lendület CMS Particle and Nuclear Physics Group, Eötvös Loránd University, Budapest, Hungary
- 21: Also at Institute of Physics, University of Debrecen, Debrecen, Hungary
- 22: Also at Indian Institute of Technology Bhubaneswar, Bhubaneswar, India
- 23: Also at Institute of Physics, Bhubaneswar, India
- 24: Also at University of Visva-Bharati, Santiniketan, India
- 25: Also at University of Ruhuna, Matara, Sri Lanka
- 26: Also at Isfahan University of Technology, Isfahan, Iran
- 27: Also at Yazd University, Yazd, Iran
- 28: Also at Plasma Physics Research Center, Science and Research Branch, Islamic Azad University, Tehran, Iran
- 29: Also at Università degli Studi di Siena, Siena, Italy
- 30: Also at INFN Sezione di Milano-Bicocca; Università di Milano-Bicocca, Milano, Italy
- 31: Also at Purdue University, West Lafayette, USA
- 32: Also at International Islamic University of Malaysia, Kuala Lumpur, Malaysia
- 33: Also at Malaysian Nuclear Agency, MOSTI, Kajang, Malaysia
- 34: Also at Consejo Nacional de Ciencia y Tecnología, Mexico city, Mexico
- 35: Also at Warsaw University of Technology, Institute of Electronic Systems, Warsaw, Poland
- 36: Also at Institute for Nuclear Research, Moscow, Russia
- 37: Now at National Research Nuclear University 'Moscow Engineering Physics Institute' (MEPhI), Moscow, Russia
- 38: Also at St. Petersburg State Polytechnical University, St. Petersburg, Russia
- 39: Also at University of Florida, Gainesville, USA
- 40: Also at P.N. Lebedev Physical Institute, Moscow, Russia
- 41: Also at California Institute of Technology, Pasadena, USA

- 42: Also at Budker Institute of Nuclear Physics, Novosibirsk, Russia
43: Also at Faculty of Physics, University of Belgrade, Belgrade, Serbia
44: Also at INFN Sezione di Roma; Sapienza Università di Roma, Rome, Italy
45: Also at University of Belgrade, Faculty of Physics and Vinca Institute of Nuclear Sciences, Belgrade, Serbia
46: Also at Scuola Normale e Sezione dell'INFN, Pisa, Italy
47: Also at National and Kapodistrian University of Athens, Athens, Greece
48: Also at Riga Technical University, Riga, Latvia
49: Also at Universität Zürich, Zurich, Switzerland
50: Also at Stefan Meyer Institute for Subatomic Physics (SMI), Vienna, Austria
51: Also at Istanbul University, Faculty of Science, Istanbul, Turkey
52: Also at Gaziosmanpasa University, Tokat, Turkey
53: Also at Istanbul Aydin University, Istanbul, Turkey
54: Also at Mersin University, Mersin, Turkey
55: Also at Cag University, Mersin, Turkey
56: Also at Piri Reis University, Istanbul, Turkey
57: Also at Adiyaman University, Adiyaman, Turkey
58: Also at Izmir Institute of Technology, Izmir, Turkey
59: Also at Necmettin Erbakan University, Konya, Turkey
60: Also at Marmara University, Istanbul, Turkey
61: Also at Kafkas University, Kars, Turkey
62: Also at Istanbul Bilgi University, Istanbul, Turkey
63: Also at Rutherford Appleton Laboratory, Didcot, United Kingdom
64: Also at School of Physics and Astronomy, University of Southampton, Southampton, United Kingdom
65: Also at Instituto de Astrofísica de Canarias, La Laguna, Spain
66: Also at Utah Valley University, Orem, USA
67: Also at Beykent University, Istanbul, Turkey
68: Also at Bingol University, Bingol, Turkey
69: Also at Erzincan University, Erzincan, Turkey
70: Also at Sinop University, Sinop, Turkey
71: Also at Mimar Sinan University, Istanbul, Istanbul, Turkey
72: Also at Texas A&M University at Qatar, Doha, Qatar
73: Also at Kyungpook National University, Daegu, Korea